AN INVESTIGATION OF THE DYNAMIC LATERAL STABILITY AND CONTROL OF A PARAWING VEHICLE

By

Joseph R. Chambers

Thesis submitted to the Graduate Faculty of the

Virginia Polytechnic Institute

in candidacy for the degree of

MASTER OF SCIENCE

in

Aerospace Engineering

May 1966

Blacksburg, Virginia

AN INVESTIGATION OF THE DYNAMIC LATERAL STABILITY AND CONTROL OF A PARAWING VEHICLE

By

Joseph R. Chambers

ABSTRACT

Parawing vehicles may have unusual values of many of the mass and aerodynamic factors affecting dynamic lateral stability and control. These unusual characteristics are due in large part to the fact that the center of gravity of parawing vehicles is located far below the parawing, whereas conventional aircraft usually have the vertical center-of-gravity location near the plane of the wings. The present thesis is an analytical investigation of the dynamic lateral stability and control of a typical parawing vehicle. The analysis was made using three-degree-of-freedom, rigid body equations of motion. Stability derivatives used in the calculations were obtained from static and dynamic force tests of a parawing model with rigid leading-edge and keel members. The analysis is treated mainly in terms of the effects of vertical center-of-gravity position, since this was found to be the most significant factor affecting the lateral stability and control of the hypothetical vehicle.

AUTHOR

AN INVESTIGATION OF THE DYNAMIC LATERAL STABILITY AND CONTROL OF A PARAWING VEHICLE

By

Joseph R. Chambers

Thesis submitted to the Graduate Faculty of the

Virginia Polytechnic Institute

in candidacy for the degree of

MASTER OF SCIENCE

in

Aerospace Engineering

APPROVED:

J. B. Eades, Jr., Chairman

F. J. Maher

Y. Kashiwagi

May 1966

Blacksburg, Virginia

II. TABLE OF CONTENTS

III. LIST OF FIGURES

IV. LIST OF TABLES

V. INTRODUCTION

A wide range of applications of the parawing concept is currently being considered. This type of wing can be packaged and deployed in a manner similar to recovery parachutes, and in addition provides attractive glide and landing flare capabilities. Some proposed uses of the concept are cargo dropping, spacecraft recovery, manned utility vehicles and rocket booster recovery. A considerable amount of aerodynamic data have been obtained in support of these applications, however, the factors affecting the stability and control of such vehicles have not been clearly defined. Most investigations of the dynamic stability and control of parawing vehicles have been of a qualitative nature using dynamically scaled free-flight models. (See refs. 1 to 4, for example.) In view of the lack of detailed analysis concerning the stability and control of parawing configurations, the present investigation was made to improve the basic understanding of the major factors influencing the stability of such vehicles. The stability and control characteristics of parawing vehicles might be expected to differ from those of conventional aircraft because certain physical characteristics of the configurations differ markedly from the characteristics of conventional aircraft. Among these physical characteristics are: (1) a center-of-gravity location far below the wing, (2) a mass distribution in which the mass is distributed mainly along a vertical axis, and (3) a wing having a shape which tends to produce large values of lateral force due to sideslip (C_{Y_β}). The second factor is a result of the first, and the

third factor is important because of the first. Since the low center-of-gravity position was expected to have a predominant influence on the dynamic lateral stability and control of a parawing vehicle, the analysis is treated mainly in terms of the effect of vertical center-of-gravity location on lateral stability. The effects of individual stability derivatives were also investigated to determine which ones were primarily responsible for the effects of center-of-gravity location on dynamic lateral stability.

The investigation consisted of a theoretical determination of the dynamic lateral characteristics of an unpowered parawing-payload combination gliding at maximum lift-drag ratio for several vertical center-of-gravity locations. Stability derivatives used in the calculations were based on the results of static and dynamic force tests of a parawing model having an aspect ratio of 2.83 and deployed leading edge sweep angle of 50°. The effects of center-of-gravity location on the stability derivatives are considered important in themselves to the understanding of the dynamic stability and control of parawing vehicles. Consequently, the effects of center-of-gravity location on the derivatives are analyzed as a distinct part of the investigation.

VI. SYMBOLS AND NOMENCLATURE

The calculated stability and control results are presented with respect to the stability axis system shown in figure 1. All basic force test data of the parawing model are presented for the body axis system shown in figure 2. The aerodynamic coefficients are based on the flat-pattern characteristics of the parawing (45° leading-edge sweep condition) given in table 1.

A,B,C,D,E	coefficients of lateral stability quartic
b	wing span, ft
$\bar{c}$	mean aerodynamic chord, ft
C_D	drag coefficient, $F_D/q_\infty S$
C_L	lift coefficient, $F_L/q_\infty S$
C_l	rolling moment coefficient, $M_X/q_\infty Sb$
ΔC_l	incremental rolling moment coefficient
C_m	pitching moment coefficient, $M_Y/q_\infty S\bar{c}$
C_n	yawing moment coefficient, $M_Z/q_\infty Sb$
ΔC_n	incremental yawing-moment coefficient
C_Y	side-force coefficient, $F_Y/q_\infty S$
ΔC_Y	incremental side-force coefficient
$C_{l/2}$	number of cycles required for the amplitude of a lateral oscillation to decrease by a factor of 2
D_b	differential operator (d/ds_b)
f	frequency of oscillation, cps
F_D	drag, lb

F_L lift, lb

F_Y side-force, lb

g acceleration due to gravity, ft/sec^2

k reduced frequency parameter, $\frac{\omega b}{2V}$

k_{X_o} radius of gyration in roll about principal longitudinal axis, ft

k_{Z_o} radius of gyration in yaw about principal vertical axis, ft

K_{X_o} nondimensional radius of gyration in roll about principal longitudinal axis (k_{X_o}/b)

K_{Z_o} nondimensional radius of gyration in yaw about principal vertical axis (k_{Z_o}/b)

K_X nondimensional radius of gyration in roll about longitudinal stability axis $\left(\sqrt{K_{X_o}^2 \cos^2\eta + K_{Z_o}^2 \sin^2\eta} \right)$

K_Z nondimensional radius of gyration in yaw about vertical stability axis $\left(\sqrt{K_{X_o}^2 \sin^2\eta + K_{Z_o}^2 \cos^2\eta} \right)$

K_{XZ} nondimensional product-of-inertia parameter $\left(\left(K_{Z_o}^2 - K_{X_o}^2 \right) \sin\eta \cos\eta \right)$

L/D lift-drag ratio

L/D_{max} maximum lift-drag ratio

m mass, slugs

M_X rolling moment, ft-lb

M_Y pitching moment, ft-lb

M_Z yawing moment, ft-lb

P	period of oscillation, sec
p	rolling velocity, rad/sec
q_∞	free-stream dynamic pressure, lb/sq ft
r	yawing velocity, rad/sec
R	Routh's discriminant
S	wing area, sq ft
s_b	nondimensional time parameter based on span (Vt/b)
t	time, sec
$t_{1/2}$	time required for the amplitude of the lateral oscillation to decrease by a factor of 2, sec
V	free-stream velocity, ft/sec
X,Y,Z	body reference axes
$\frac{x}{b}, \frac{z}{b}$	nondimensional distances along the body reference axes from basic moment reference center (see fig. 3)
$\frac{\bar{x}}{b}, \frac{\bar{z}}{b}$	nondimensional distances measured from 0.5 keel length station to center-of-gravity location measured in axis system parallel to stability axes (see fig. 1)
x_i	any of the mass or aerodynamic terms in the lateral equations of motion
α	angle of attack of keel, deg
β	angle of sideslip, deg or rad
$\dot{\beta}$	rate of change of sideslip, rad/sec
β_w	angle of sideslip of parawing, deg
γ	flight path angle (see fig. 1), deg

ϵ angle between reference axis and principal axis, positive when reference axis is above principal axis at nose, deg (see fig. 1)

η angle of attack of principal longitudinal axis, positive when principal axis is above flight path at the nose (fig. 1), deg

λ root of stability quartic $A\lambda^4 + B\lambda^3 + C\lambda^2 + D\lambda + E = 0$

μ_b lateral relative-density factor ($m/\rho Sb$)

ρ mass density of air, slugs/cu ft

σ ratio of air density at altitude to that at sea level

ϕ angle of bank, deg or rad

ϕ_w angle of bank of parawing, positive when right wing tip is down, deg

ψ angle of yaw, deg or rad

$\left|\frac{\phi}{\psi}\right|$ ratio of the amplitudes of roll and yaw present in a mode of motion

$\left|\frac{\phi}{\beta}\right|$ ratio of the amplitudes of roll and sideslip present in a mode of motion

$\left|\frac{\phi}{V_e}\right|$ rolling parameter, $\frac{57.3}{V\sigma}\left|\frac{\phi}{\beta}\right|$ deg/ft/sec

$\omega = 2\pi f$, radians/sec

$C_{l_\beta} = \frac{\partial C_l}{\partial \beta}$, per deg or per rad

$C_{n_\beta} = \frac{\partial C_n}{\partial \beta}$, per deg or per rad

$C_{Y_\beta} = \frac{\partial C_Y}{\partial \beta}$, per deg or per rad

$$C_{l_p} = \frac{\partial C_l}{\partial \frac{pb}{2V}} \qquad C_{n_p} = \frac{\partial C_n}{\partial \frac{pb}{2V}} \qquad C_{Y_p} = \frac{\partial C_Y}{\partial \frac{pb}{2V}}$$

$$C_{l_{\dot{p}}} = \frac{\partial C_l}{\partial \frac{\dot{p}b^2}{4V^2}} \qquad C_{n_{\dot{p}}} = \frac{\partial C_n}{\partial \frac{\dot{p}b^2}{4V^2}} \qquad C_{Y_{\dot{p}}} = \frac{\partial C_Y}{\partial \frac{\dot{p}b^2}{4V^2}}$$

$$C_{l_r} = \frac{\partial C_l}{\partial \frac{rb}{2V}} \qquad C_{n_r} = \frac{\partial C_n}{\partial \frac{rb}{2V}} \qquad C_{Y_r} = \frac{\partial C_Y}{\partial \frac{rb}{2V}}$$

$$C_{l_{\dot{r}}} = \frac{\partial C_l}{\partial \frac{\dot{r}b^2}{4V^2}} \qquad C_{n_{\dot{r}}} = \frac{\partial C_n}{\partial \frac{\dot{r}b^2}{4V^2}} \qquad C_{Y_{\dot{r}}} = \frac{\partial C_Y}{\partial \frac{\dot{r}b^2}{4V^2}}$$

In the present investigation the term "in-phase derivative" refers to any one of the oscillatory derivatives that is based on the components of forces and moments in phase with the angular displacement during the oscillatory tests. The term "out-of-phase derivative" refers to any one of the stability derivatives that is based on the components of forces and moments 90° out of phase with angular displacement. The oscillatory derivatives of the present investigation were measured in the following combinations:

Rolling Oscillation Tests

$$\left.\begin{aligned} &C_{l_\beta} \sin\alpha - k^2 C_{l_{\dot{p}}} \\ &C_{n_\beta} \sin\alpha - k^2 C_{n_{\dot{p}}} \\ &C_{Y_\beta} \sin\alpha - k^2 C_{Y_{\dot{p}}} \end{aligned}\right\} \quad \text{In-phase}$$

$$\left.\begin{aligned} &C_{l_p} + C_{l_{\dot{\beta}}} \sin \alpha \\ &C_{n_p} + C_{n_{\dot{\beta}}} \sin \alpha \\ &C_{Y_p} + C_{Y_{\dot{\beta}}} \sin \alpha \end{aligned}\right\} \text{Out-of-phase}$$

Yawing Oscillation Tests

$$\left.\begin{aligned} &C_{l_\beta} \cos \alpha + k^2 C_{l_{\dot{r}}} \\ &C_{n_\beta} \cos \alpha + k^2 C_{n_{\dot{r}}} \\ &C_{Y_\beta} \cos \alpha + k^2 C_{Y_{\dot{r}}} \end{aligned}\right\} \text{In-phase}$$

$$\left.\begin{aligned} &C_{l_r} - C_{l_{\dot{\beta}}} \cos \alpha \\ &C_{n_r} - C_{n_{\dot{\beta}}} \cos \alpha \\ &C_{Y_r} - C_{Y_{\dot{\beta}}} \cos \alpha \end{aligned}\right\} \text{Out-of-phase}$$

VII. ANALYSIS

A. Method of Analysis

The analysis was made for a hypothetical paraglider system consisting of a parawing-payload combination having the mass characteristics of a recently proposed recovery system. The parawing and payload were assumed to be rigidly joined so that there was no relative motion between them except for intentional control movements. Longitudinal trim was assumed to be obtained solely by varying the fore and aft position of the center of gravity of the system. The vertical center-of-gravity location was varied by locating the payload relative to the parawing in such a manner as to yield several specified center-of-gravity locations perpendicular to the parawing keel member (in terms of z/b) while maintaining the proper position parallel to the keel (in terms of x/b) required for longitudinal trim. The stability derivatives for each center-of-gravity location were then estimated from measured derivatives for the wing alone, and calculations were made to determine the dynamic lateral stability and control of the vehicle for each center-of-gravity location.

B. Description of Vehicle

The recovery system was assumed to employ an aspect-ratio 2.83 parawing having a conical canopy and flat-pattern sweep angle of 45°. In the deployed, or flight condition the parawing fabric was supported in a 50° sweep condition by three rigid tubular members which formed the keel and leading edges of the parawing. Parawing and payload weights

were 400 pounds and 3400 pounds, respectively. The payload aerodynamics were assumed to consist only of drag and were considered only in the determination of longitudinal trim. The system center-of-gravity location was varied in the previously discussed manner such that three different configurations of the original concept were studied. These configurations are herein referred to as A, B, and C, (z/b = 0.25, 0.50, and 0.75, respectively).

The configurations were assumed to use the wing-bank system for lateral control - that is, the wing was banked about an axis parallel to the keel member to produce the forces and moments required for lateral control. This is, in effect, similar to the center-of-gravity shift type of control actually used on parawings with suspended payloads. As stated in reference 3, when such a system is used for control the incremental lateral force and moment coefficients produced by wing bank may approximately be expressed as

$$\left.\begin{aligned} \Delta C_Y &= C_{Y_\beta}\ \beta_w + C_L \sin \phi_w \\ \Delta C_n &= C_{n_\beta}\ \beta_w + \frac{\bar{x}}{b} C_L \sin \phi_w \\ \Delta C_l &= C_{l_\beta}\ \beta_w + \frac{\bar{z}}{b} C_L \sin \phi_w \end{aligned}\right\} \qquad (1)$$

where $\sin \beta_w = \sin \alpha \sin \phi_w$.

The first terms of the right hand side of the equations arise from the fact that a value of sideslip is obtained at the parawing when the wing is banked for keel angles of attack other than zero. The second terms are the contributions of the lateral component of the lift vector which has been tilted by banking the wing.

C. Determination of Stability Derivatives

The lateral stability derivatives of the configurations were assumed to be due to the parawing alone. There was virtually no information available on the dynamic stability derivatives, however; so, in order to provide reasonable inputs for the dynamic stability analysis, an experimental investigation was conducted to determine both the static and dynamic stability derivatives of a 0.15-scale model of the parawing assumed for the theoretical analysis.

A sketch of the model parawing is presented in figure 3. The model was constructed of nonporous plastic membrane attached to three equal length rigid members such that in the deployed or flight condition the rigid members supported the fabric in a 50° sweep condition. Additional information pertaining to the model can be found in reference 5.

The static and dynamic force tests were conducted in a low-speed tunnel with a 12-foot octogonal test section at the Langley Research Center. The tests were made at a dynamic pressure of 1.63 pounds per square foot which corresponds to a Reynolds number of 0.99×10^6 based on the keel length. The static lateral tests were made for an angle-of-sideslip range of $\pm 5^{\circ}$. Forced oscillation tests were made in yaw and roll with angular amplitudes of $\pm 5^{\circ}$ and for a value of the reduced frequency parameter k of 0.25. A detailed description of the dynamic force test equipment and the method of obtaining the dynamic parameters is presented in reference 6. The moments were all measured about the basic moment center shown in figure 3; and the static and dynamic lateral stability derivatives of the complete configurations were

obtained by transferring these measured wing-alone model data to the required center-of-gravity locations by means of the equations of reference 7 which are included in the appendix of this paper for convenience.

D. Method and Scope of Calculations

Calculations were made to determine the dynamic lateral stability and control of the three parawing configurations for the condition of L/D_{max} gliding flight at an altitude of 10,000 feet.

The lateral stability calculations consisted of the determination of the damping and period of the lateral modes of motion. The damping of both the oscillatory and aperiodic modes is expressed in terms of the damping factor $\frac{1}{t_{1/2}}$, the reciprocal of the time to damp to one-half amplitude. Positive values of this parameter indicate stability (positive damping) and negative values indicate instability (negative damping). The calculations were made using the equations of motion given in appendix B. Stability boundaries in terms of the dihedral effect derivative C_{l_β} and the directional stability derivative C_{n_β} were also determined. The spiral, or static stability boundary is described by

$$E = 0 \tag{2}$$

while the necessary and sufficient conditions for neutral oscillatory stability are that the coefficients of the stability quartic satisfy Routh's discriminant set equal to zero

$$R = BCD - AD^2 - B^2E = 0 \tag{3}$$

and that B and D have the same sign. The significance of the lateral stability boundaries is indicated by a discussion of the modes of motion in the C_{l_β}, C_{n_β} plane.

Calculations were also made to determine which aerodynamic and mass parameters affected the lateral stability of the configurations to the greatest extent as the center-of-gravity location was varied. These calculations were made using the method of reference 8 which is based on a Taylor's series expansion of the roots of the stability quartic near the original solution. Although strictly applicable only for small incremental changes in derivatives and mass parameters near the original solution, the method does afford an insight as to the important terms in the equations of motion as the center of gravity and hence the stability derivatives and mass distribution are changed. The results are presented as slopes indicating the rate of change of the damping and frequency of the various modes of the lateral motion with changes in any of the parameters in the equations of motion.

In conjunction with these calculations, the graphical root locus technique was used to help visualize the character of the solution of the lateral stability quartic as the mass and aerodynamic parameters were varied. This method illustrates the path, or locus of the solutions of the quartic on the complex plane. Presented in figure 4 are the features of the complex plane as applied to dynamic systems. Lines of constant time to halve amplitude (or double amplitude) are parallel to the imaginary axis. Radial lines emanating from the origin represent constant values of damping ratios and cycles to halve (or

double amplitude. Circles with centers at the origin represent lines of constant undamped natural frequency. For stability, all roots of the quartic must be located in the left half of the complex plane; that is, there must be no positive real parts to the solutions.

The lateral control calculations consisted of calculation of the lateral motions following a step input of 5° wing-bank angle. The equations of motion were solved using numerical integration techniques in conjunction with a digital computer.

All of the foregoing types of calculations were made for configurations A, B, and C. In an attempt to provide a better understanding of the magnitude of the factors causing the effects of vertical center-of-gravity position shown by comparison of the results for configurations A, B, and C, additional calculations were made for configuration A in which the values of mass and aerodynamic parameters were changed one-at-a-time to the values for configuration B to determine the effects of these individual parameter changes on damping and period.

VIII. RESULTS AND DISCUSSION

A. Presentation of Results

The results of the parawing model force tests are presented in figures 5 to 8. Calculated lateral stability derivatives and mass characteristics of the three full-scale configurations are presented in figures 9 to 12 and are tabulated in table 2. The results of the dynamic lateral stability calculations are presented in figures 13 through 18 with the sensitivity of the dynamic lateral stability of the configurations to changes in the stability derivatives and mass parameters being listed in tables 3 and 4. Root locus plots showing the changes in the character of the solutions of the lateral stability quartic as the stability and mass parameters are changed are presented in figures 19 to 28. Time histories of the motions following wing-bank input are presented in figures 29 and 30. The two primary results of the investigation - the changes in the stability derivatives and mass parameters with center-of-gravity location and the effects on dynamic lateral stability and control of these parameter changes - are discussed separately.

It should be noted that any theoretical analysis of the dynamics of a parawing configuration can be limited by the concept itself. The flexibility of the parawing, the means of connection between parawing and payload, and the number of degrees of freedom of the system all complicate and in some cases may render useless any analytic attempt to predict the dynamics of the system. Consequently, the calculated

results contained herein do not apply directly to parawing configurations or flight conditions other than those investigated. It is believed, however, that the major results and trends shown by these calculations are indicative of the dynamic characteristics to be expected of vehicles which have the following characteristics: very low center-of-gravity location, mass distributed mainly along the vertical axis, and a wing which has a large value of the lateral-force derivative C_{Y_β}. These characteristics are typical of a wide variety of paragliders, or gliding parachutes.

B. Stability Derivatives and Mass Parameters

Mass distribution.- The calculated mass and geometric characteristics of the three configurations are given in table 2. It should be noted that for all three configurations the nondimensional radius of gyration in roll (K_X) was larger than the nondimensional radius of gyration in yaw (K_Z). This situation is quite different from that of a conventional airplane where the radius of gyration in roll is less than that in yaw ($K_X < K_Z$) and leads to near-vertical inclinations of the principal axis of least inertia. This difference would be expected to lead to substantial differences in the character of the lateral motions between parawing vehicles and conventional aircraft. For example, the large values of inclination of the axis of least inertia will lead to increased yawing components in the lateral modes of motion since a vehicle will inherently tend to move about an axis of least inertia.

It whould be noted that in the present investigation, the principal longitudinal axis (the axis to which η is referenced) was considered,

in the conventional manner, to be the axis located in a generally forward direction. The only unusual situation was that for the parawing vehicles this was the axis of greatest inertia.

Longitudinal characteristics.- The parawing system was assumed (on the basis of the model force test data of figure 5 with an added drag increment to account for the payload) to have a maximum L/D value of 4.27 at 25° keel angle of attack for all center-of-gravity locations. The longitudinal stability of the configurations was not investigated in this study, but it might be noted that a paraglider configuration becomes more stable longitudinally for increasing values of x/b and z/b.

Static lateral stability derivatives.- The static lateral stability characteristics of the parawing model are presented in figure 6 in the form of the static stability derivatives C_{Y_β}, C_{n_β}, and C_{l_β} plotted against angle of attack. The values of the derivatives were obtained from the differences between the values of the coefficients at sideslip angles of +5° and -5°. The variation of C_{n_β} (referenced to body axes) shows a negative, or destabilizing trend at about 33° angle of attack. It should not be inferred from this result that a vehicle with this parawing would experience a directional divergence at these higher angles of attack. It is a well established fact that when an aircraft has large negative values of C_{l_β} in conjunction with the negative values of C_{n_β} a directional divergence does not necessarily occur. This point is discussed in detail in reference 9.

The values of the static lateral stability derivatives (referenced to stability axes) for the three configurations based on the model data and the transfer equations of the appendix are given in figure 9. Lowering the center-of-gravity location from configuration A to that of configuration C increased the values of both C_{n_β} and $-C_{l_\beta}$. The increase in the directional stability derivative C_{n_β} is caused by the fact that as vertical center-of-gravity location ($\bar{z}/b$) is increased, the horizontal location ($\bar{x}/b$) must also be changed to maintain longitudinal trim.

Dynamic lateral stability derivatives.- The variation of the in-phase oscillatory derivatives with angle of attack for the parawing model is presented in figure 7. Static data referenced to body axes are also presented and are shown to be generally in good agreement with the oscillatory data.

The variation of the out-of-phase derivatives with angle of attack is presented in figure 8. The damping-in-roll parameter ($C_{l_p} + C_{l_{\dot\beta}} \sin \alpha$) and the damping-in-yaw parameter ($C_{n_r} - C_{n_{\dot\beta}} \cos \alpha$) were essentially constant over the angle-of-attack range up to the stall, which probably indicates that the $\dot\beta$ portion of the derivatives were negligible in the angle-of-attack range below about 35°. This apparent lack of $\dot\beta$ derivatives is in contrast with results of forced oscillation tests of swept rigid wings (see ref. 10, for example) in which separated flow effects have led to large values of the $\dot\beta$ derivatives at high angles of attack. The contrasting characteristics of the parawing may have been caused by the flexibility of the parawing itself or by leading-

edge characteristics. In any event, it was assumed that the rate-of-change of sideslip ($\dot{\beta}$) derivatives were negligible and the measured combinations were treated as pure rolling and yawing derivatives in the dynamic stability calculations. For example, the combination $C_{l_p} + C_{l_{\dot{\beta}}} \sin \alpha$ was assumed to be C_{l_p} for purposes of determining the lateral stability derivatives of the full-scale configuration.

The calculated effect of center-of-gravity location on the dynamic lateral stability derivatives of the three full-scale parawing configurations is shown in figures 10 and 11. Lowering the center-of-gravity location from that of configuration A to configuration C led to a positive increase in the yawing moment due to rolling velocity (C_{n_p}) and negative increases in the damping in roll derivative (C_{l_p}) and the damping in yaw derivative (C_{n_r}). The changes in the dynamic stability derivatives with vertical center-of-gravity location are quite large because of the combination of large distance between the center of gravity and the wing and large lateral-force derivative C_{Y_β} which enter into the transfer of these derivatives as products. In effect, increasing the vertical distance between the center of gravity and the parawing keel essentially makes the parawing act as a high vertical tail (with short tail length) would on a conventional airplane - that is, the side-force derivative C_{Y_β} of the parawing tends to be the predominant contributor to the derivative transfer equations.

The incremental values of lateral force and moment coefficients produced by 5° wing-bank angle as calculated from equations (1) are presented in figure 12. The incremental rolling moment coefficient

ΔC_l is increased by lowering the center-of-gravity position. The yawing moment increment is negative, or adverse, for all configurations.

C. Dynamic Lateral Stability and Control

The results of the calculations to determine dynamic lateral stability are discussed in terms of the stability of the different modes of lateral motion. For conventional aircraft, these modes are usually a highly damped aperiodic rolling motion known as the roll subsidence mode, a lightly damped aperiodic motion involving yawing and rolling known as the spiral mode, and a lateral oscillation known as the Dutch roll. Although the lateral modes of the parawing configurations may be different in nature in comparison with conventional nomenclature will be used to identify the various modes.

Location of roots on the complex plane.- The nondimensional roots of the lateral stability quartic for each configuration are plotted on the complex plane in figure 13. The two aperiodic (real) roots are negative and both are therefore stable. Of particular interest is the relatively light damping of the roll mode for these configurations. The complex pairs representing the lateral oscillation are near the neutral stability line, indicating low values of damping. The damping ratios for configurations A, B, and C are 0.0128, 0.0968, and 0.166, respectively.

Stability boundaries.- Lateral dynamic stability boundaries for the configurations are presented as functions of C_{l_β} and C_{n_β} in figure 14. All configurations are located in a region of the plane

where stability exists, as has been previously pointed out by the complex plane representation. Increasing the directional stability derivative C_{n_β} will lead to spiral instability for both configurations A and B, however, configuration C is spirally stable for all positive values of C_{n_β}. Increasing $-C_{l_\beta}$ leads to oscillatory instability in all configurations. An inspection of the root locus sketches of figure 21 shows that in the case of configuration A, the Dutch roll roots cross over into the right half of the complex plane and become unstable for increasing dihedral effect. The oscillatory instability which occurs in configurations B and C is the result of the roll and spiral roots combining to form a long period oscillation.

Roll subsidence mode.- The calculated damping factor of the roll subsidence mode of the configurations is presented in figure 15. The data indicate that the system became less damped as the center-of-gravity location of the system was moved downward from that of configuration A to that of configuration C. The dashed line represents the classical single degree of freedom approximation to the roll subsidence mode damping $\left(\frac{1}{t_{1/2}} = \frac{C_{l_p} V}{1.57\ \mu_b\ K_X^2 b}\right)$ which generally gives a reasonably accurate approximation for conventional aircraft. Comparison of the two results indicates large differences between the complete three degree of freedom results and the simple single degree of freedom results. This result indicates that the damping of this mode of motion is dependent on factors other than those included in the simple approximation.

The calculated variation in the damping factor of the roll subsidence mode with changes in the various parameters in the equations of motion are presented in table 3. Positive values of $\frac{\partial \frac{1}{t_{1/2}}}{\partial x_i}$ together with positive increases in x_i (or negative values of $\frac{\partial \frac{1}{t_{1/2}}}{\partial x_i}$ together with negative increases in x_i) lead to positive (stabilizing) increases in the damping of this particular mode of motion. The results show that the yawing moment derivatives and inertia parameters can appreciably affect the damping of this mode. The results of the additional calculations in which the parameters in the equations of motion of configuration A were changed one at a time to those of configuration B in an effort to determine the relative magnitude of the changes in the roll mode damping due to changes in mass and aerodynamic parameters are presented in table 4 together with results predicted by the slope method. The results show that the decrease in damping of the roll mode as the center-of-gravity location changed from that of configuration A to configuration B was caused primarily by the destabilizing contributions of the derivative C_{n_p} and the mass parameter K_X^2. The increased importance of the yawing derivatives in the determination of the damping of the roll mode can be explained by the data of figure 16 which presents the ratio of roll to yaw amplitude in the roll mode. Values of this parameter usually are in the range of 30 to 100 for conventional aircraft but for these parawing configurations with their associated stability parameters, all values were below 5 and indicate the mode was not a pure rolling motion

but involved relatively large yawing motions. In fact, for the lower center-of-gravity location (configuration C), the motion consisted of almost an equal rolling and yawing - which is quite different from the case for conventional aircraft where the motion is almost pure rolling.

Spiral mode.- The calculated results presented in figure A indicate that the spiral mode became slightly more damped as the center of gravity was lowered with respect to the wing. An inspection of table 4 indicates that the stabilizing effect was primarily due to the stabilizing influence of changes in those derivatives (C_{l_β} and C_{n_r}) that usually affect the spiral stability of an aircraft. The spiral root can usually be approximated by $\lambda = -\frac{E}{D}$ and those terms which most affect this ratio are seen to be of great importance in the damping of the spiral mode for the parawing configuration - as they have traditionally been for conventional airplanes.

Oscillatory mode.- Presented in figures 17 and 18 are summaries of the Dutch roll oscillation characteristics of the three configurations. The inverse cyclic damping $\frac{1}{C_{l/2}}$ and roll to sideslip parameter $\left|\frac{\phi}{v_e}\right|$ for each configuration are presented together with the recommended boundary of reference 11 in figure 17. The presentation of the Dutch roll characteristics in this manner is not necessarily meant to imply that parawing configurations should conform to the handling quality parameters of conventional aircraft, but it is one of the present standards available for evaluating the effect of the Dutch roll characteristics on flying qualities and is consequently used for purposes of comparison. The results are also compared in figure 18 to

the older handling quality requirements (expressed in terms of damping and period of the oscillation) of reference 12 inasmuch as the present day aircraft requirements tend to present pessimistic views of the oscillatory characteristics of vehicles having extremely light wing loadings (the equivalent side velocity v_e of such vehicles is much smaller than that of conventional aircraft). The results indicate that increasing the vertical distance between parawing and payload (varying center-of-gravity location from configuration A to C) led to a longer period, better damped lateral oscillation, and smaller values of roll-to-sideslip ratio. Only configuration C satisfied the present day handling quality requirements with both configurations A and B lacking satisfactory Dutch roll damping. The results presented in figure 18 show that only configuration A did not satisfy the older handling quality requirements.

Tables 3 and 4 indicate that the increase in damping as the center of gravity is lowered is primarily caused by the stabilizing contribution resulting from the positive increase in C_{n_p} being larger than the destabilizing contribution of K_{XZ}. The effects of C_{n_p} on the damping of the lateral oscillation and aperiodic modes have been investigated in the past (refs. 13 and 14) where it was shown that positive increases in the derivative usually increases the damping of the Dutch roll mode while decreasing the damping of the roll subsidence mode. The derivative C_{n_p} will almost always be increased positively by increasing vertical distance between the parawing and center of gravity. Increases in the same geometric variables will usually lead to negative values of K_{XZ} as explained previously.

It should be noted that in table 3 the contributions of C_{n_β}, C_{l_β}, and C_{l_β} to the Dutch roll damping reverse signs between configurations A and B. That is, increases in the derivatives in the usual stabilizing sense (negative for C_{l_p}, positive for C_{n_β} and C_{l_β}) lead to less stable Dutch roll oscillations for configurations B and C. An examination of the root locus sketches of figures 20 and 21 reveals that the location of the circular symbols (zeros) change between configuration A and B. This changes the nature of the solution of the stability quartic; for example, in figure 21 the Dutch roll mode rapidly becomes unstable as dihedral effect is increased for configuration A while the mode becomes more stable for configurations B and C. These results are primarily due to the effect of C_{n_p} on the distribution of damping of the system. Similar results are reported in reference 13 for large positive values of C_{n_p}. As discussed in reference 14, the total damping of the system can be expressed as B/A. The partial derivative of the ratio with respect to any parameter x_i must therefore follow the relation

$$\frac{V}{0.693\ b}\frac{\partial\frac{B}{A}}{\partial x_i} = \left(\frac{\partial\frac{1}{t_{1/2}}}{\partial x_i}\right)_{\substack{\text{Spiral}\\ \text{mode}}} + \left(\frac{\partial\frac{1}{t_{1/2}}}{\partial x_i}\right)_{\substack{\text{Roll}\\ \text{mode}}} + 2\left(\frac{\partial\frac{1}{t_{1/2}}}{\partial x_i}\right)_{\substack{\text{Dutch roll}\\ \text{mode}}}$$

Since $\frac{\partial\frac{B}{A}}{\partial x_i}$ for C_{n_β} and C_{l_β} must be zero (changes in these derivatives do not change the total damping but merely redistribute the damping among the modes) the stabilizing contribution of the derivatives to the roll subsidence damping (as in configuration A) is accompanied by a decrease in the Dutch roll damping.

Theoretical investigations in the past (see ref. 15, for example) have shown that the reversal of the sign of $\left(\frac{\partial \frac{1}{t_{1/2}}}{\partial C_{l_\beta}}\right)_{\substack{\text{Dutch roll} \\ \text{mode}}}$ between configurations A and B could be predicted by the algebraic sign of the expression

$$C_{n_p} - 2C_L K_Z^2$$

Positive values of this quantity indicated that increases in the effective dihedral parameter $-C_{l_\beta}$ would lead to larger values of the Dutch roll damping factor. The reversal of the sense of the contribution of C_{l_β} to the damping of the lateral oscillation as the center-of-gravity was lowered with respect to the parawing was therefore due to the positive increase in C_{n_p} brought about by center-of-gravity position.

The data presented in tables 3 and 4 indicate that the decrease in frequency of the Dutch roll oscillation with increasing values of $\bar{x}/b$ was due primarily to the mass parameters K_{XZ} and K_X^2 and the stability derivatives C_{n_β}, C_{n_p}, and C_{l_β}.

The effect of increasing the raduis of gyration in yaw as presented in figure 28 should be noted inasmuch as the root locus shows the Dutch roll mode becomes unstable for increases in yawing inertia. This fact may be important for parawing configurations having large values of yawing moment of inertia, such as parawing-booster combinations.

Lateral response to wing-bank control.- The responses of the configuration to 5° wing-bank control are presented in figure 29. The

results of the three-degree-of-freedom calculations show that the initial roll response was about equal for all configurations; but, as the motion progressed, the configurations with the lower center-of-gravity locations (configurations B and C) showed greater response to wing-bank control. The enlarged plot of the time history of the initial yawing motions shown in figure 30 indicates that increasing the vertical center-of-gravity location decreased the initial adverse yawing motion, which is opposite to what would be expected from a static aerodynamic standpoint. This result is caused by the favorable contribution of the product-of-inertia factor to the initial yawing acceleration as expressed by the relation:

$$D_b^2\psi = \frac{\Delta C_n - \frac{K_{XZ}}{K_X^2}\Delta C_l}{2K_Z^2\mu_b\left(1 - \frac{K_{XZ}^2}{K_X^2 K_Z^2}\right)} \tag{4}$$

As pointed out in reference 16 and as can be seen from equation (4), negative values of K_{XZ} give a favorable yawing moment contribution and can thereby significantly affect the yawing characteristics in an aileron roll as the center-of-gravity location is lowered from that of configuration A to that of configuration C. The product of inertia parameter, as discussed earlier, will almost certainly be negative for large values of z/b.

IX. CONCLUSIONS

The results of a theoretical investigation of the dynamic lateral stability and control of a parawing configuration having rigid leading edge and keel members may be summarized as follows:

1. Increasing the vertical distance between the center of gravity and the parawing keel while maintaining the horizontal location required for longitudinal trim led to a decrease in the damping of the roll-subsidence mode and an increase in the damping of the spiral mode. Lowering the center of gravity also caused an increase in the damping and period of the lateral oscillation and a reduction in the ratio of roll to sideslip.

2. The two parameters that most affected the damping of the lateral oscillation with vertical changes in center of gravity location were the yawing-moment-due-to-rolling derivative C_{n_p} and the nondimensional product of inertia factor K_{XZ}.

3. There was little effect of vertical center-of-gravity location on the initial roll response to wing bank control but as the motion progressed the configurations having the lower centers of gravity displayed the greater roll response. The effects of vertical center of gravity location on the mass distribution of the system produced significant changes in the initial adverse yawing motion following the application of wing bank control. Negative values of K_{XZ} caused by lowering the center of gravity relative to the parawing tended to reduce the initial adverse yaw.

X. ACKNOWLEDGMENTS

The author wishes to express his appreciation to the National Aeronautics and Space Administration for the permission to use the material in this thesis which was obtained from a research project at the Langley Research Center.

He also wishes to thank Dr. James B. Eades, Jr., of the Aerospace Engineering Department for his assistance in preparing this thesis.

XI. REFERENCES

1. Shanks, Robert E.: Experimental Investigation of the Dynamic Stability of a Towed Parawing Glider Air Cargo Delivery System. NASA TN D-2292, 1964.

2. Burk, Sanger M., Jr.: Free-Flight Investigation of the Deployment, Dynamic Stability, and Control Characteristics of a 1/12-Scale Dynamic Radio-Controlled Model of a Large Booster and Parawing. NASA TN D-1932, 1963.

3. Johnson, Joseph L., Jr.: Low-Speed Force and Flight Investigation of a Model of a Modified Parawing Utility Vehicle. NASA TN D-2492, 1965.

4. Hewes, Donald E.: Free-Flight Investigation of Radio-Controlled Models With Parawings. NASA TN D-927, 1961.

5. Polhamus, Edward C.; and Naeseth, Rodger L.: Experimental and Theoretical Studies of the Effects of Camber and Twist on the Aerodynamic Characteristics of Parawings Having Nominal Aspect Ratios of 3 and 6. NASA TN D-972, 1963.

6. Hewes, Donald E.: Low-Subsonic Measurements of the Static and Oscillatory Lateral Stability Derivatives of a Sweptback-Wing Airplane Configuration at Angles of Attack From -10° to 90°. NASA Memo 5-20-59L, 1959.

7. Babister, A. W.: Aircraft Stability and Control. Vol. I of Flight Testing, div. VI, International Series of Monographs in Aeronautics and Astronautics, M. C. Wilson, ed., Pergamon Press, 1961.

8. Gates, Ordway, Jr.; and Woodling, C. H.: A Method for Estimating Variations in the Roots of the Lateral-Stability Quartic Due to Changes in Mass and Aerodynamic Parameters of an Airplane. NACA TN 3134, 1954.

9. Moul, Martin T.; and Paulson, John W.: Dynamic Lateral Behavior of High-Performance Aircraft. NACA RM L58E16, 1958.

10. Campbell, John P.; Johnson, Joseph L., Jr.; and Hewes, Donald E.: Low-Speed Study of the Effect of Frequency on the Stability Derivatives of Wings Oscillating in Yaw with Particular Reference to High Angle-of-Attack Conditions. NACA RM L55H05, 1955.

11. Anon: Flying Qualities of Piloted Airplanes. MIL-F-8785 (ASG), Sept. 1, 1954, Amendment - 4, Apr. 17, 1959.

12. Anon: Flying Qualities of Piloted Airplanes. USAF Spec. 1815-B, June 1, 1948.

13. Johnson, Joseph L.; and Sternfield, Leonard: A Theoretical Investigation of the Effect of Yawing Moment Due to Rolling on Lateral Oscillatory Stability. NACA TN 1723, 1948.

14. Schade, Robert O.; and Hassell, James L., Jr.: The Effects on Dynamic Lateral Stability and Control of Large Artificial Variations in the Rotary Stability Derivatives. NACA Report 1151, 1953. (Supercedes NACA TN 2781, 1952.)

15. Sternfield, Leonard; and Gates, Ordway B., Jr.: A Simplified Method for the Determination and Analysis of the Neutral-Lateral Stability Boundary. NACA Report 943, 1949. (Supercedes NACA TN 1727, 1948.)

16. Hewes, Donald E.: The Effects of Mass Distribution on the Low-Speed Dynamic Lateral Stability and Control Characteristics of a Model with a 45° Sweptback Wing. NACA TN 2313, 1951.

XII. VITA

The author was born in Houma, Louisiana, on October 13, 1940. He graduated from Lafayette Senior High School in Lafayette, Louisiana, in 1958. In September 1958, he entered the Georgia Institute of Technology in Atlanta, Georgia, where he received the degree of Bachelor of Science in Aeronautical Engineering in June 1962. Since that time the author has been employed by the National Aeronautics and Space Administration at Langley Research Center, Langley Station, Hampton, Virginia.

J. R. Chambers

XIII. APPENDICES

A. Stability Derivative Transfer Equations

The distances x and z correspond to those of figure 3. Zero subscripts indicate data measured about the basic reference center

$$C_{Y_\beta} = C_{Y_{\beta_o}}$$

$$C_{Y_p} = C_{Y_{p_o}} \cos\alpha + C_{Y_{r_o}} \sin\alpha + 2C_{Y_{\beta_o}} \left(\frac{z}{b}\cos\alpha - \frac{x}{b}\sin\alpha\right)$$

$$C_{Y_r} = C_{Y_{r_o}} \cos\alpha - C_{Y_{p_o}} \sin\alpha - 2C_{Y_{\beta_o}} \left(\frac{x}{b}\cos\alpha + \frac{z}{b}\sin\alpha\right)$$

$$C_{l_\beta} = C_{l_{\beta_o}} \cos\alpha + C_{n_{\beta_o}} \sin\alpha + C_{Y_\beta}\left(\frac{z}{b}\cos\alpha - \frac{x}{b}\sin\alpha\right)$$

$$C_{l_p} = C_{l_{p_o}} \cos^2\alpha + \left(C_{l_{r_o}} + C_{n_{p_o}}\right)\sin\alpha\cos\alpha + C_{n_{r_o}} \sin^2\alpha$$

$$+ \left[\left(C_{Y_{p_o}} + 2C_{l_{\beta_o}}\right)\cos\alpha + \left(C_{Y_{r_o}} + 2C_{n_{\beta_o}}\right)\sin\alpha\right]\left[\frac{z}{b}\cos\alpha - \frac{x}{b}\sin\alpha\right]$$

$$+ 2C_{Y_{\beta_o}}\left[\frac{z}{b}\cos\alpha - \frac{x}{b}\sin\alpha\right]^2$$

$$C_{l_r} = C_{l_{r_o}} \cos^2\alpha + \left(C_{n_{r_o}} - C_{l_{p_o}}\right)\sin\alpha\cos\alpha - C_{n_{p_o}} \sin^2\alpha$$

$$- \frac{x}{b}\left[2C_{l_{\beta_o}} \cos^2\alpha + \left(C_{Y_{r_o}} + 2C_{n_{\beta_o}}\right)\sin\alpha\cos\alpha - C_{Y_{p_o}} \sin^2\alpha\right]$$

$$+ \frac{z}{b}\left[C_{Y_{r_o}} \cos^2\alpha - \left(C_{Y_{p_o}} + 2C_{l_{\beta_o}}\right)\sin\alpha\cos\alpha - 2C_{n_{\beta_o}} \sin^2\alpha\right]$$

$$+ 2C_{Y_{\beta_o}}\left[\left(\frac{x^2}{b^2} - \frac{z^2}{b^2}\right)\sin\alpha\cos\alpha - \frac{xz}{b}\left(\cos^2\alpha - \sin^2\alpha\right)\right]$$

$$C_{n_\beta} = C_{n_{\beta_o}} \cos\alpha - C_{l_{\beta_o}} \sin\alpha - C_{Y_{\beta_o}}\left(\frac{x}{b}\cos\alpha + \frac{x}{b}\sin\alpha\right)$$

$$C_{n_p} = C_{n_{p_o}} \cos^2\alpha + \left(C_{n_{r_o}} - C_{l_{p_o}}\right)\sin\alpha\cos\alpha - C_{l_{r_o}} \sin^2\alpha$$

$$- \frac{x}{b}\left[C_{Y_{p_o}} \cos^2\alpha + \left(C_{Y_{r_o}} + 2C_{n_{\beta_o}}\right)\sin\alpha\cos\alpha - 2C_{l_{\beta_o}} \sin^2\alpha\right]$$

$$+ \frac{z}{b}\left[2C_{n_{\beta_o}} \cos^2\alpha - C_{Y_{p_o}} + 2C_{l_{\beta_o}} \sin\alpha\cos\alpha - C_{Y_{r_o}} \sin^2\alpha\right]$$

$$+ 2C_{Y_{\beta_o}}\left[\left(\frac{x^2}{b^2} - \frac{z^2}{b^2}\right)\sin\alpha\cos\alpha - \frac{xz}{b^2}\left(\cos^2\alpha - \sin^2\alpha\right)\right]$$

$$C_{n_r} = C_{n_{r_o}} \cos^2\alpha - \left(C_{l_{r_o}} + C_{n_{p_o}}\right)\sin\alpha\cos\alpha + C_{l_{p_o}} \sin^2\alpha$$

$$- \left(C_{Y_{r_o}} + 2C_{n_{\beta_o}}\right)\cos\alpha - \left(C_{Y_{p_o}} + 2C_{l_{\beta_o}}\right)\sin\alpha\left[+ \frac{x}{b}\cos\alpha + \frac{z}{b}\sin\alpha\right]$$

$$+ 2C_{Y_{\beta_o}}\left(- \frac{x}{b}\cos\alpha - \frac{z}{b}\sin\alpha\right)^2$$

B. Equations of Motion

The nondimensional lateral equations of motion referred to a stability-axes system (fig. 1), are:

Roll

$$2\mu_b\left(K_X^2 D_b^2\phi + K_{XZ} D_b^2\psi\right) = C_{l_\beta}\beta + \frac{1}{2} C_{l_p} D_b\phi + \frac{1}{2} C_{l_r} D_b\psi$$

Yaw

$$2\mu_b\left(K_Z^2 D_b^2\psi + K_{XZ} D_b^2\phi\right) = C_{n_\beta}\beta + \frac{1}{2} C_{n_p} D_b\phi + \frac{1}{2} C_{n_r} D_b\psi$$

Sideslip

$$2\mu_b\left(D_b\beta + D_b\psi\right) = C_{Y_\beta}\beta + \frac{1}{2} C_{Y_p} D_b\phi + C_L\phi + \frac{1}{2} C_{Y_r} D_b\psi + \left(C_L \tan\gamma\ \psi\right)$$

When $\phi_o e^{\lambda s_b}$ is substituted for ϕ, $\psi_o e^{\lambda s_b}$ for ψ, and $\beta_o e^{\lambda s_b}$ for β in the equations written in determinant form, λ must be a root of the stability equation

$$A\lambda^4 + B\lambda^3 + C\lambda^2 + D\lambda + E = 0 \qquad (1)$$

where

$$A = 8\mu_b^3\left(K_X^2 K_Z^2 - K_{XZ}^2\right)$$

$$B = -2\mu_b^2\left(2K_X^2 K_Z^2 C_{Y_\beta} + K_X^2 C_{n_r} + K_Z^2 C_{l_p} - 2K_{XZ}^2 C_{Y_\beta} - K_{XZ} C_{l_r} - K_{XZ} C_{n_p}\right)$$

$$C = \mu_b\left(K_X^2 C_{n_r} C_{Y_\beta} + 4\mu_b K_X^2 C_{n_\beta} + K_Z^2 C_{l_p} C_{Y_\beta} + \frac{1}{2} C_{n_r} C_{l_p} - K_{XZ} C_{l_r} C_{Y_\beta}\right.$$
$$\left. - 4\mu_b K_{XZ} C_{l_\beta} - C_{n_p} K_{XZ} C_{Y_\beta} - \frac{1}{2} C_{n_p} C_{l_r} + K_{XZ} C_{n_\beta} C_{Y_p} - K_Z^2 C_{Y_p} C_{l_\beta}\right.$$
$$\left. - K_Z^2 C_{Y_r} C_{n_\beta} + K_{XZ} C_{Y_r} C_{l_\beta}\right)$$

$$D = -\frac{1}{4} C_{n_r} C_{l_p} C_{Y_\beta} - \mu_b C_{l_p} C_{n_\beta} + \frac{1}{4} C_{n_p} C_{l_r} C_{Y_\beta} + \mu_b C_{n_p} C_{l_\beta} + 2\mu_b C_L K_{XZ} C_{n_\beta}$$

$$- 2\mu_b C_L K_Z^2 C_{l_\beta} - 2\mu_b K_X^2 C_{n_\beta} C_L \tan\gamma + 2\mu_b K_{XZ} C_{l_\beta} C_L \tan\gamma$$

$$+ \frac{1}{4} C_{l_p} C_{n_\beta} C_{Y_r} - \frac{1}{4} C_{n_p} C_{l_\beta} C_{Y_r} - \frac{1}{4} C_{l_r} C_{n_\beta} C_{Y_p} + \frac{1}{4} C_{n_r} C_{l_\beta} C_{Y_p}$$

$$E = \frac{1}{2} C_L \left(C_{n_r} C_{l_\beta} - C_{l_r} C_{n_\beta} \right) + \frac{1}{2} C_L \tan\gamma \left(C_{l_p} C_{n_\beta} - C_{n_p} C_{l_\beta} \right)$$

The damping and period of a mode of motion in seconds are given, respectively, by the equations $t_{1/2} = -\frac{0.69}{c} \frac{b}{V}$ and $P = \frac{2\pi}{d} \frac{b}{V}$ where c and d are the real and imaginary parts of the root of the stability equation.

TABLE 1. GEOMETRIC CHARACTERISTICS OF THE MODEL

Aspect ratio	
Flat	2.83
Deployed	2.57
Area	
Flat, sq ft	12.27
Deployed, sq ft	11.16
Mean aerodynamic chord	
Flat and deployed, in.	33.33
Span	
Flat, in.	70.71
Deployed, in.	64.28
Root chord, in.	50.00
Sweep angle	
Flat, deg	45.00
Deployed, deg	50.00

TABLE 2. MASS AND AERODYNAMIC PARAMETERS

OF THE CONFIGURATIONS

	A	B	C
C_{Y_β}	-0.2556	-0.2556	-0.2556
C_{n_β}	.072165	.08275	.09325
C_{l_β}	-.14287	-.208458	-.27405
C_{Y_p}	.0701	-.06107	-.1923
C_{Y_r}	.00314	.02422	.04529
C_{l_p}	-.08946	-.17846	-.33479
C_{l_r}	.03054	.04852	.07725
C_{n_p}	.009	.0486	.09898
C_{n_r}	-.01757	-.02452	-.0332
K_X^2	.01815	.04118	.079694
K_Z^2	.0163	.01697	.018045
K_{XZ}	.000681	-.003266	-.00972
μ_b	3.183	3.183	3.183
C_L	.757	.757	.757
tan γ	-.2338	-.2338	-.2338
η	-18°12'	7°36'	9°12'
x/b	-.0636	-.1348	-.2060
z/b	.25	.50	.75

(All values are presented with respect to stability axes)

TABLE 3.- VARIATION OF THE LATERAL STABILITY OF THE THREE CONFIGURATIONS WITH CHANGES IN THE STABILITY PARAMETERS

x_i	Spiral	Roll subsidence	Dutch roll	
	$\partial \frac{1}{t_{1/2}} / \partial x_i$	$\partial \frac{1}{t_{1/2}} / \partial x_i$	$\partial \frac{1}{t_{1/2}} / \partial x_i$	$\partial \omega / \partial x_i$
Configuration A				
C_{l_p}	-0.24	-14.059	-0.97	-0.13
C_{n_p}	-0.47	-20.82	11.012	-4.88
C_{Y_p}	0.00021	-0.18	0.091	0.11
C_{l_r}	-3.77	3.36	0.55	0.20
C_{n_r}	-7.45	4.97	-7.81	1.46
C_{Y_r}	0.0034	0.043	-0.023	-0.079
C_{l_β}	-0.67	-1.23	0.95	-0.83
C_{n_β}	-1.32	-1.82	1.56	13.88
C_{Y_β}	0.00059	-0.016	-0.29	0.0034
γ	-0.25	-0.089	0.17	-0.017
K_X^2	-0.062	-85.36	1.87	-7.63
K_Z^2	-1.92	30.18	-24.81	-60.69
K_{XZ}	-1.091	-106.045	77.57	89.41
Configuration B				
C_{l_p}	-0.029	-9.22	0.10	-0.11
C_{n_p}	-0.074	-21.34	10.011	-2.56
C_{Y_p}	0.000023	-0.099	0.050	0.089
C_{l_r}	-4.26	4.55	-0.84	0.013
C_{n_r}	-10.74	10.52	-8.70	1.32
C_{Y_r}	0.0034	0.049	-0.026	-0.078
C_{l_β}	-0.95	2.052	-0.55	1.51
C_{n_β}	-2.38	4.65	-1.13	16.35
C_{Y_β}	0.00076	0.022	-0.31	-0.0042
γ	-0.17	-0.50	0.33	-0.044
K_X^2	-0.010	-33.83	2.54	6.65
K_Z^2	-3.69	38.61	-26.91	-57.82
K_{XZ}	-1.49	-61.62	44.78	59.82
Configuration C				
C_{l_p}	0.29	-6.57	1.12	0.096
C_{n_p}	0.86	-18.88	7.95	-0.86
C_{Y_p}	-0.00017	-0.046	0.023	0.066
C_{l_r}	-5.36	5.93	-1.36	-0.16
C_{n_r}	-15.74	17.064	-9.39	0.73
C_{Y_r}	0.0026	0.042	-0.022	-0.079
C_{l_β}	-1.77	5.15	-1.69	2.32
C_{n_β}	-5.13	14.48	-4.68	17.50
C_{Y_β}	0.00092	0.035	-0.35	-0.0091
γ	0.019	-1.045	0.51	-0.027
K_X^2	0.13	-14.43	0.52	7.45
K_Z^2	-6.89	37.49	-23.94	-58.095
K_{XZ}	-1.97	-28.45	23.58	39.97

TABLE 4.- VARIATION OF THE LATERAL STABILITY OF CONFIGURATION A WITH CHANGES IN THE STABILITY PARAMETERS*

K_X^2	K_Z^2	K_{XZ}	C_{l_β}	C_{n_β}	C_{Y_p}	C_{l_p}	C_{n_p}	C_{Y_r}	C_{l_r}	C_{n_r}	Spiral	Roll subsidence	Dutch roll	
											$\Delta \frac{1}{t_{1/2}}$	$\Delta \frac{1}{t_{1/2}}$	$\Delta\omega$	$\Delta \frac{1}{t_{1/2}}$
0.04118	0.01630	0.00068	-0.14287	0.07216	0.07010	-0.08946	0.00900	0.00314	0.03054	-0.01757	-0.0014	-0.93	-0.081	0.059
											(-.0014)	(-1.97)	(-.18)	(.043)
.01815	.01697	.00068	-.14287	.07216	.07010	-.08946	.00900	.00314	.03054	-.01757	-.0013	.020	-.039	-.016
											(-.0013)	(.020)	(-0.41)	(-.017)
.01815	.01630	-.00327	-.14287	.07216	.07010	-.08946	.00900	.00314	.03054	-.01757	.0045	.51	-.30	-.31
											(.0043)	(.42)	(-.35)	(-.31)
.01815	.01630	.00068	-.20846	.07216	.07010	-.08946	.00900	.00314	.03054	-.01757	.040	.078	.054	-.059
											(.044)	(.081)	(.055)	(-.062)
.01815	.01630	.00068	-.14287	.08271	.07010	-.08946	.00900	.00314	.03054	-.01757	-.013	-.018	.14	.015
											(-.014)	(-.019)	(.15)	(.016)
.01815	.01630	.00068	-.14287	.07216	-.06107	-.08946	.00900	.00314	.03054	-.01757	-.000037	.024	-.015	-.012
											(-.000028)	(.024)	(-.015)	(-.012)
.01815	.01630	.00068	-.14287	.07216	.07010	-.17846	.00900	.00314	.03054	-.01757	.012	1.29	-.0046	.073
											(.021)	(1.25)	(.011)	(.086)
.01815	.01630	.00068	-.14287	.07216	.07010	-.08946	.04860	.00314	.03054	-.01757	-.051	-1.02	-.15	.55
											(-.019)	(-.83)	(-.19)	(.44)
.01815	.01630	.00068	-.14287	.07216	.07010	-.08946	.00900	.02422	.03054	-.01757	.000062	.00072	-.0017	-.00050
											(.000070)	(.00092)	(-.0017)	(-.00049)
.01815	.01630	.00068	-.14287	.07216	.07010	-.08946	.00900	.00314	.04852	-.01757	-.065	.058	.0036	.0097
											(-.068)	(.060)	(.0036)	(.0098)
.01815	.01630	.00068	-.14287	.07216	.07010	-.08946	.00900	.00314	.03054	-.02452	.053	-.037	-.011	.054
											(.051)	(-.035)	(-.010)	(.054)

*Derivatives changed one at a time to the values for configuration B. Derivatives changed are underlined. Variations predicted by the slope method of reference 8 are indicated in parentheses.

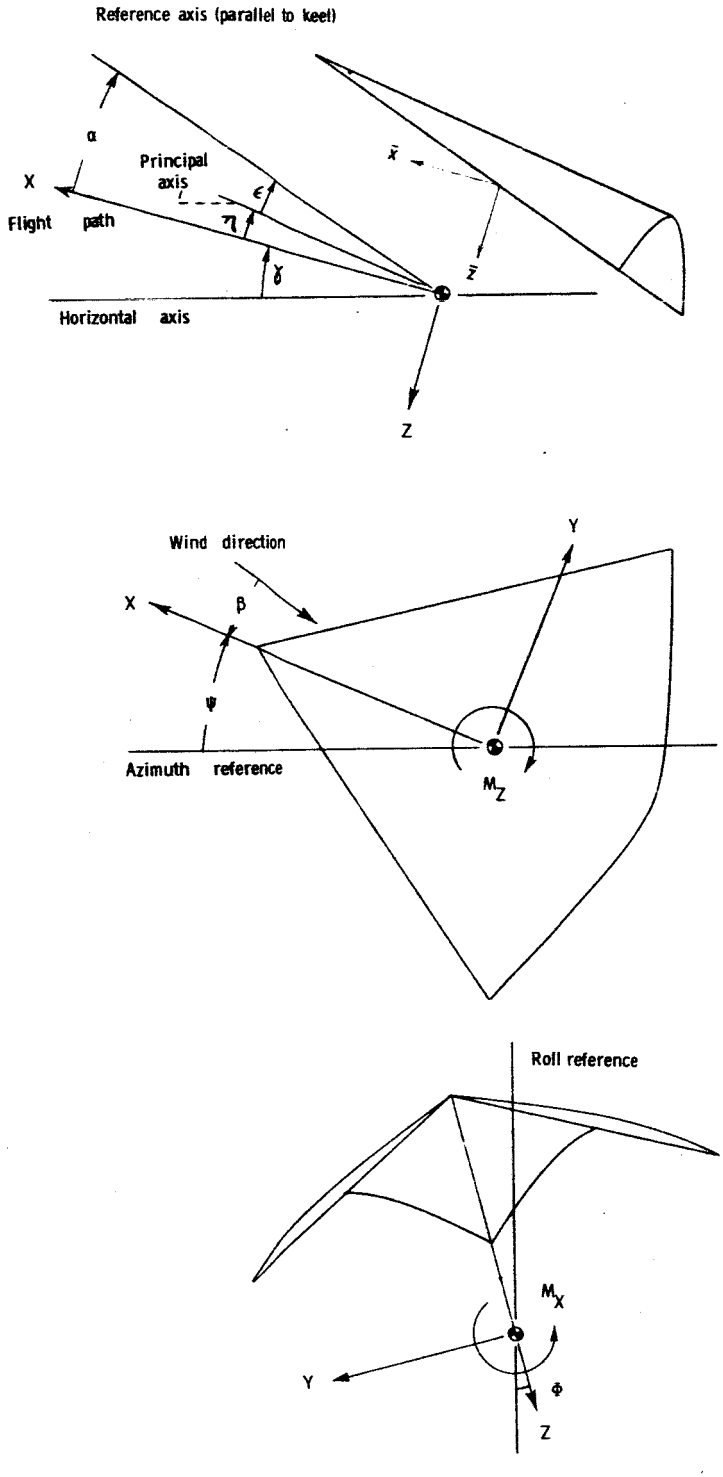

Figure 1.- The stability system of axes.

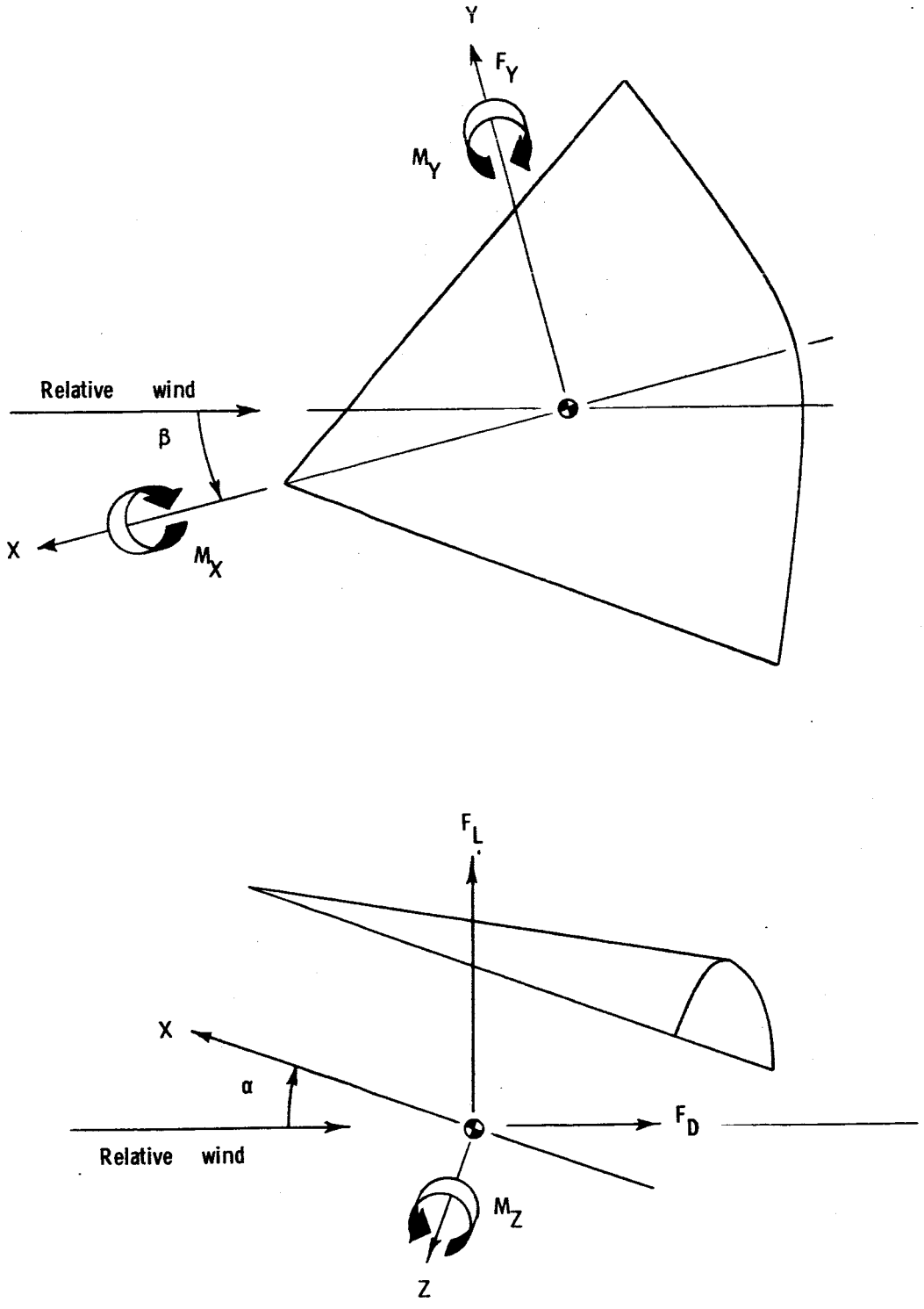

Figure 2.- The body system of axes.

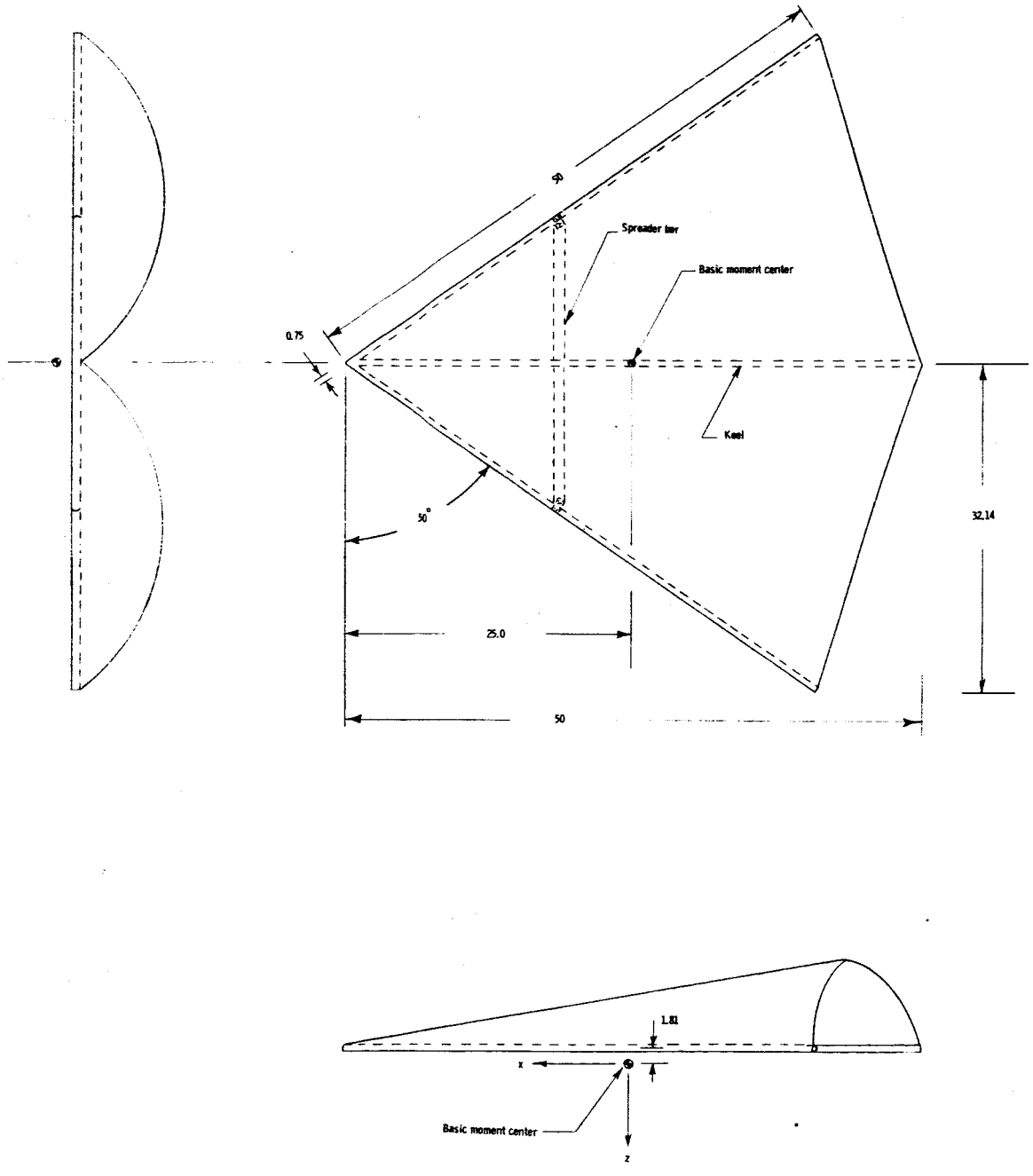

Figure 3.- Geometry of the deployed parawing model. Dimensions are given in inches.

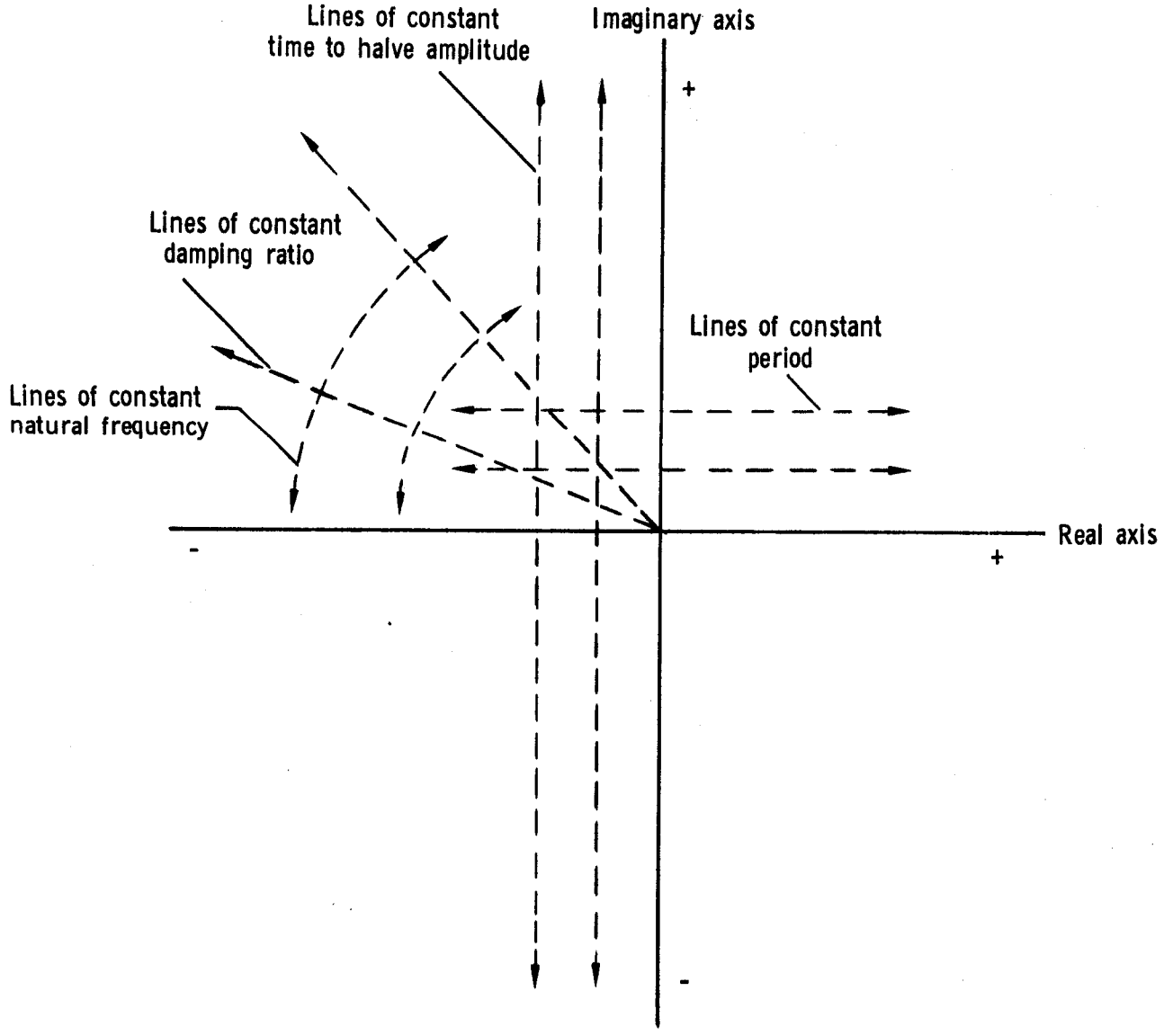

Figure 4.- Features of the complex plane.

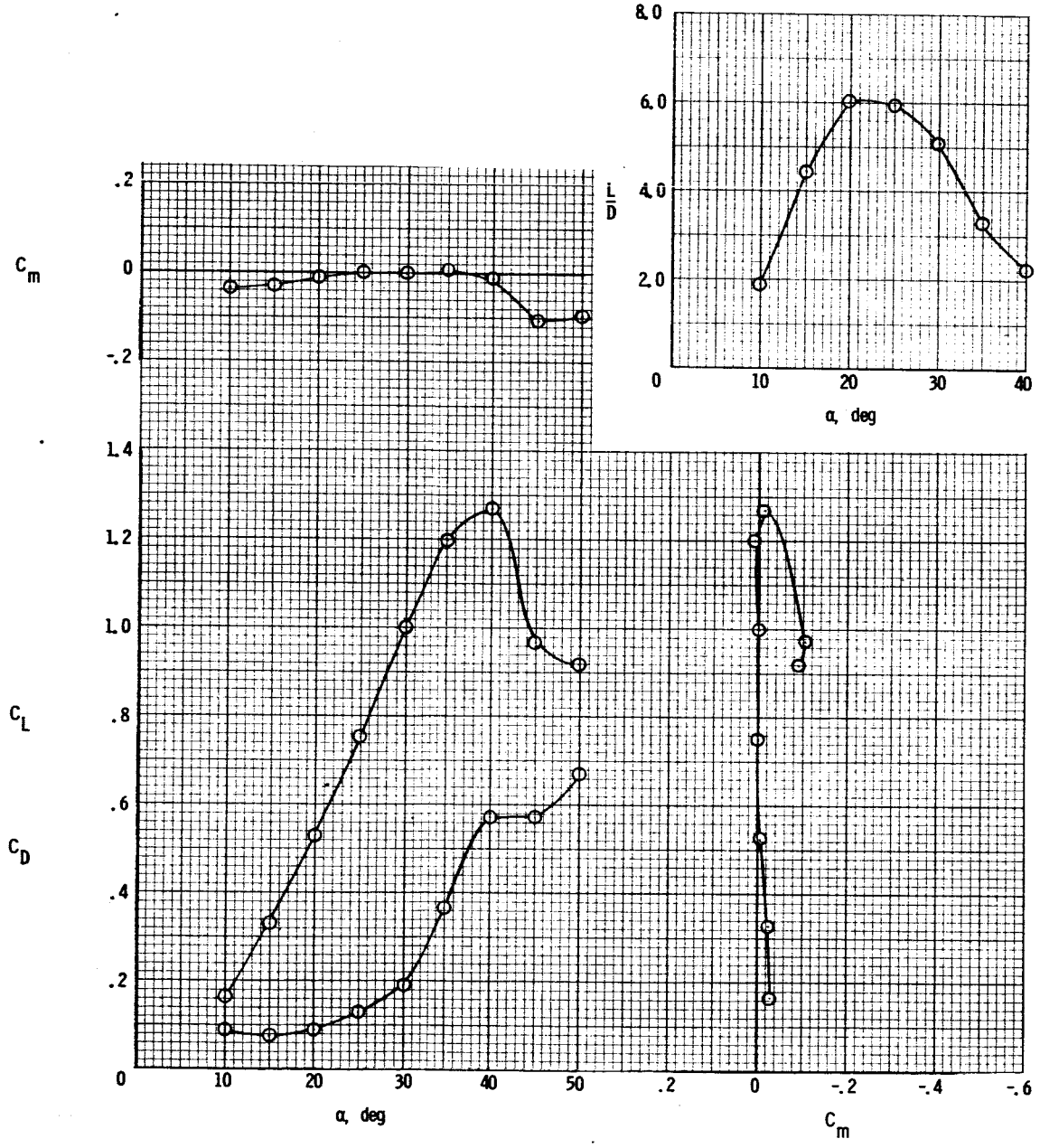

Figure 5.- Summary of the static longitudinal characteristics of the model parawing.

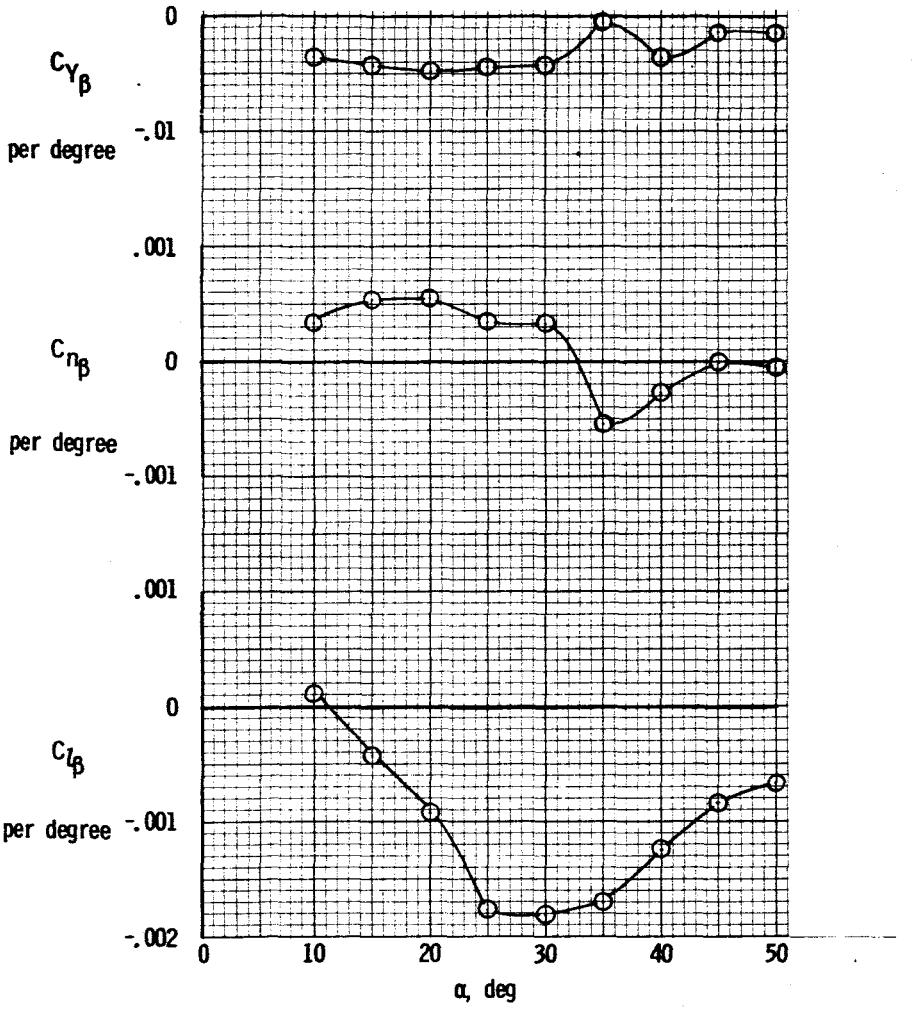

Figure 6.- Variation of the static lateral stability derivatives of the model parawing with angle of attack. Data referenced to body axes.

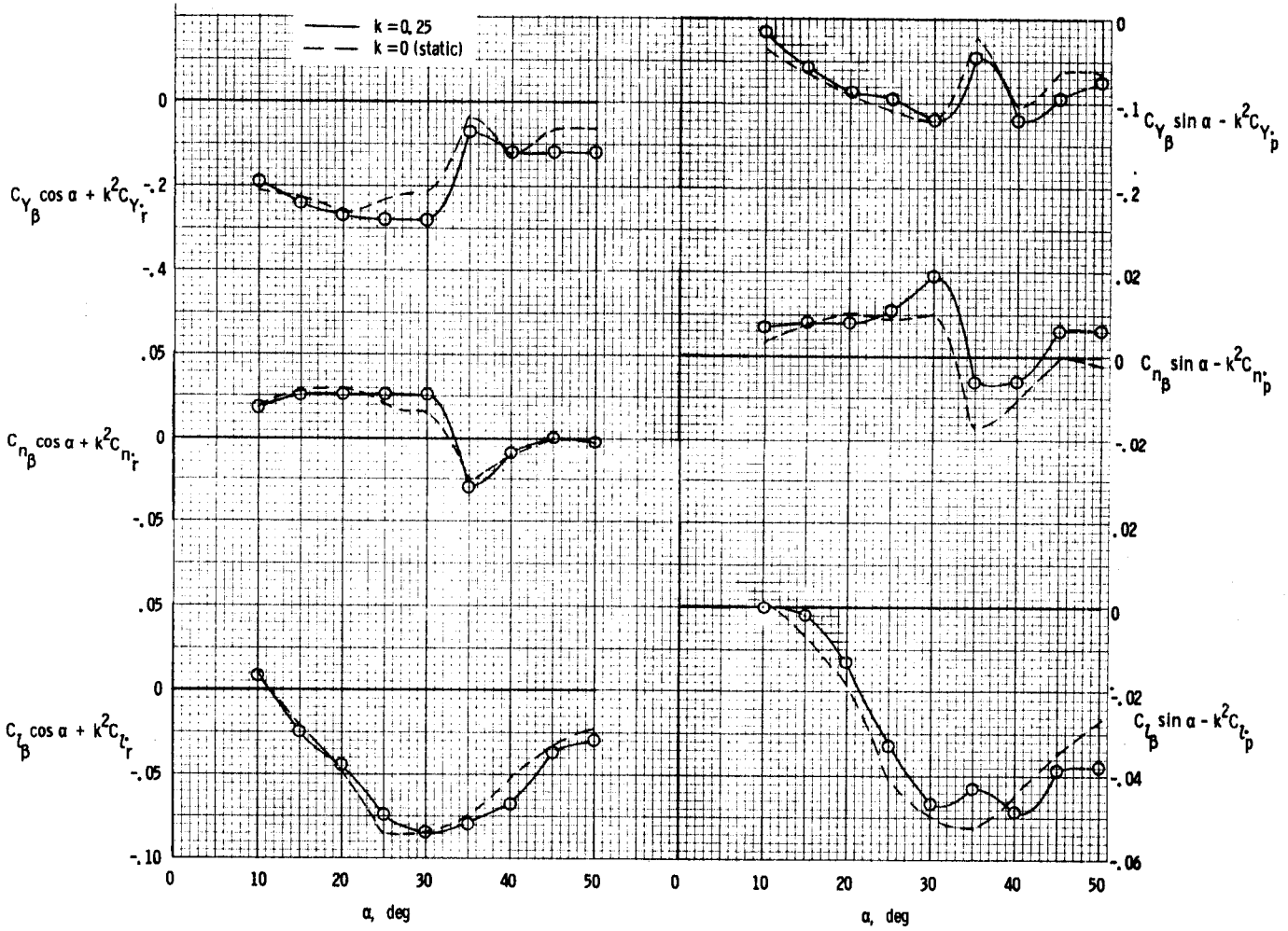

(a) Yawing.

(b) Rolling.

Figure 7.- Variation of the in-phase oscillatory derivatives with angle of attack. Data referenced to body axes.

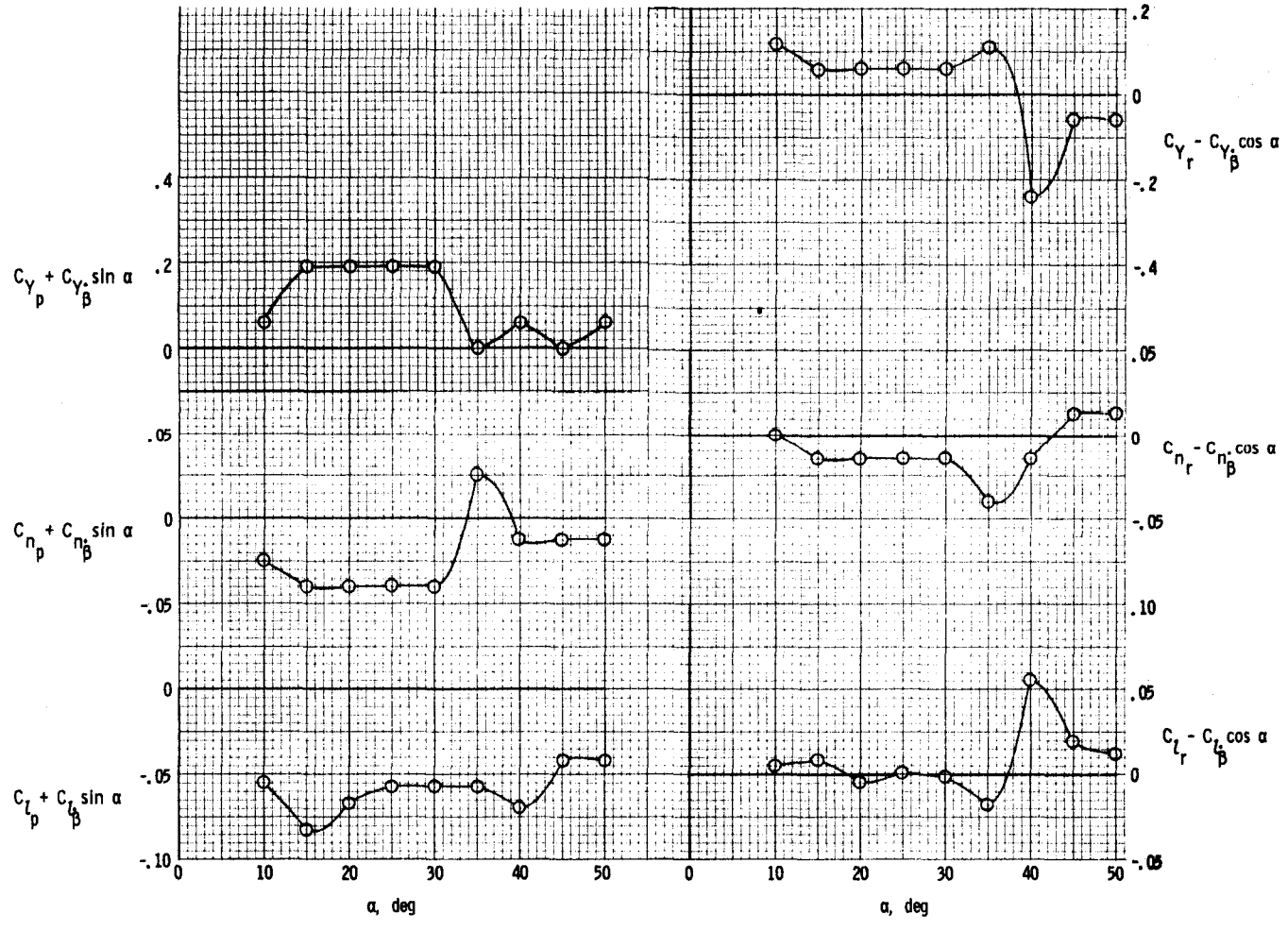

(a) Rolling.

(b) Yawing.

Figure 8.- Variation of the out-of-phase oscillatory derivatives with angle of attack. Data referenced to body axes.

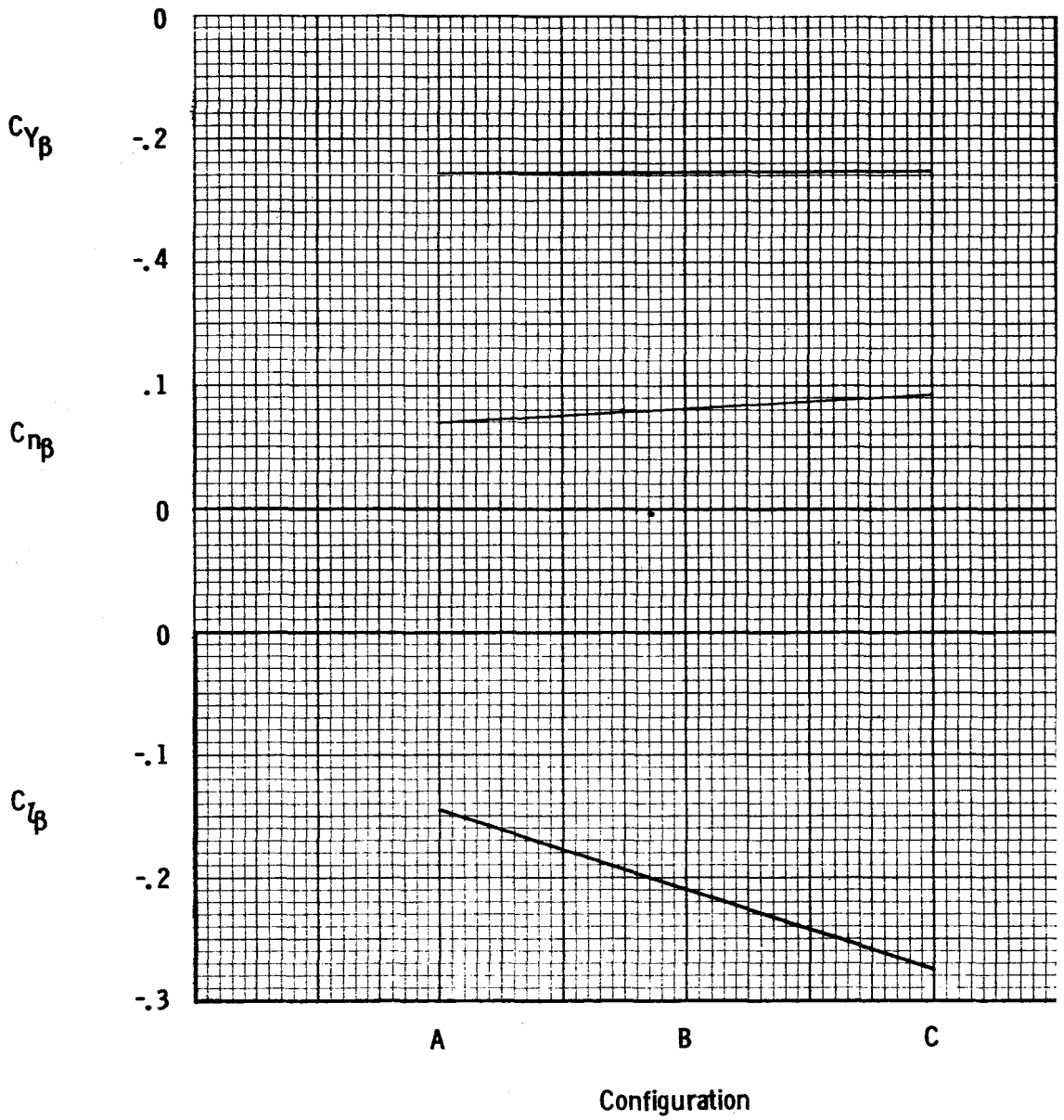

Figure 9.- Variation of the static lateral stability derivatives with center-of-gravity position. Data referenced to stability axes.

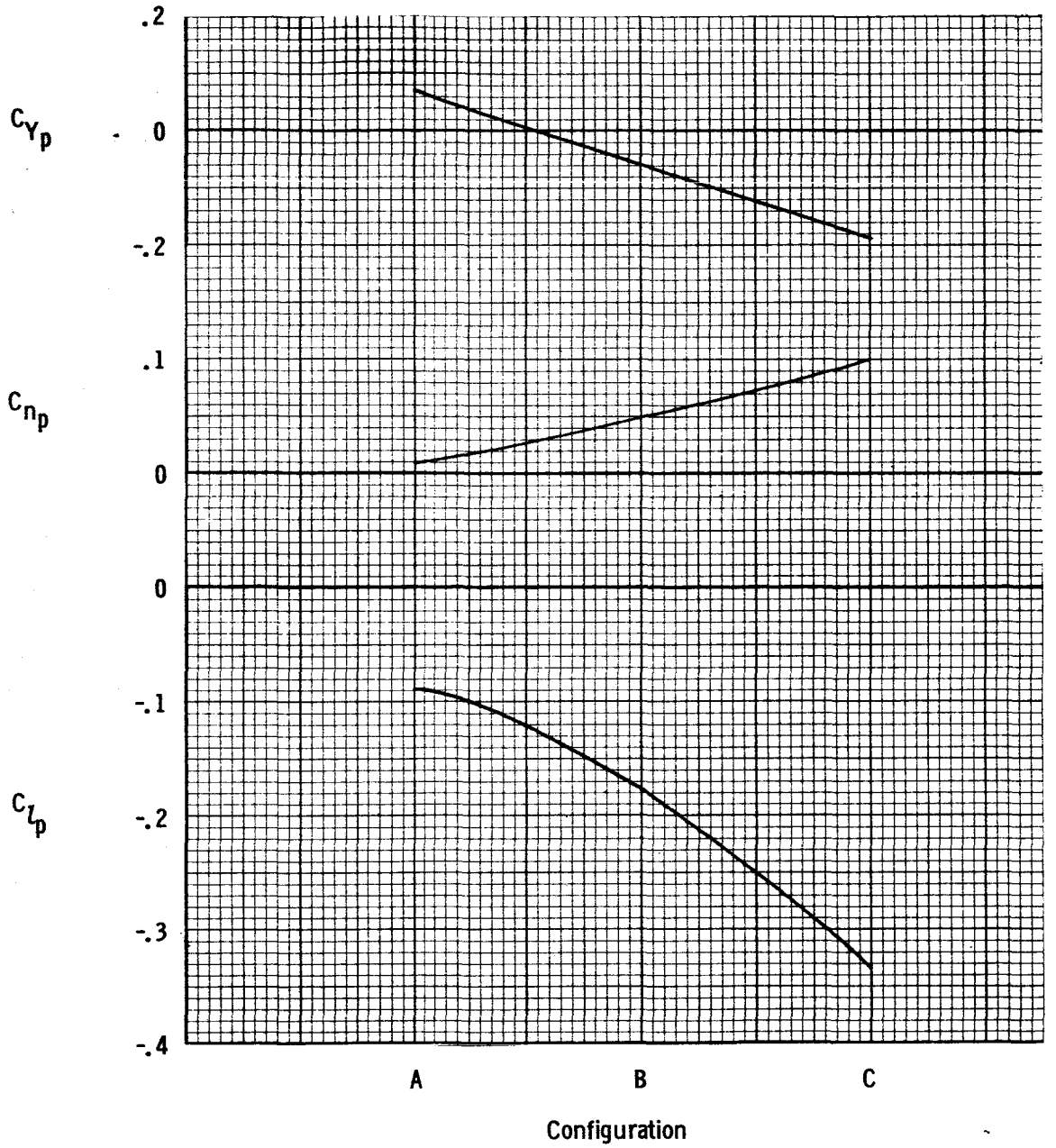

Figure 10.- Variation of the rolling lateral stability derivatives with center-of-gravity position.

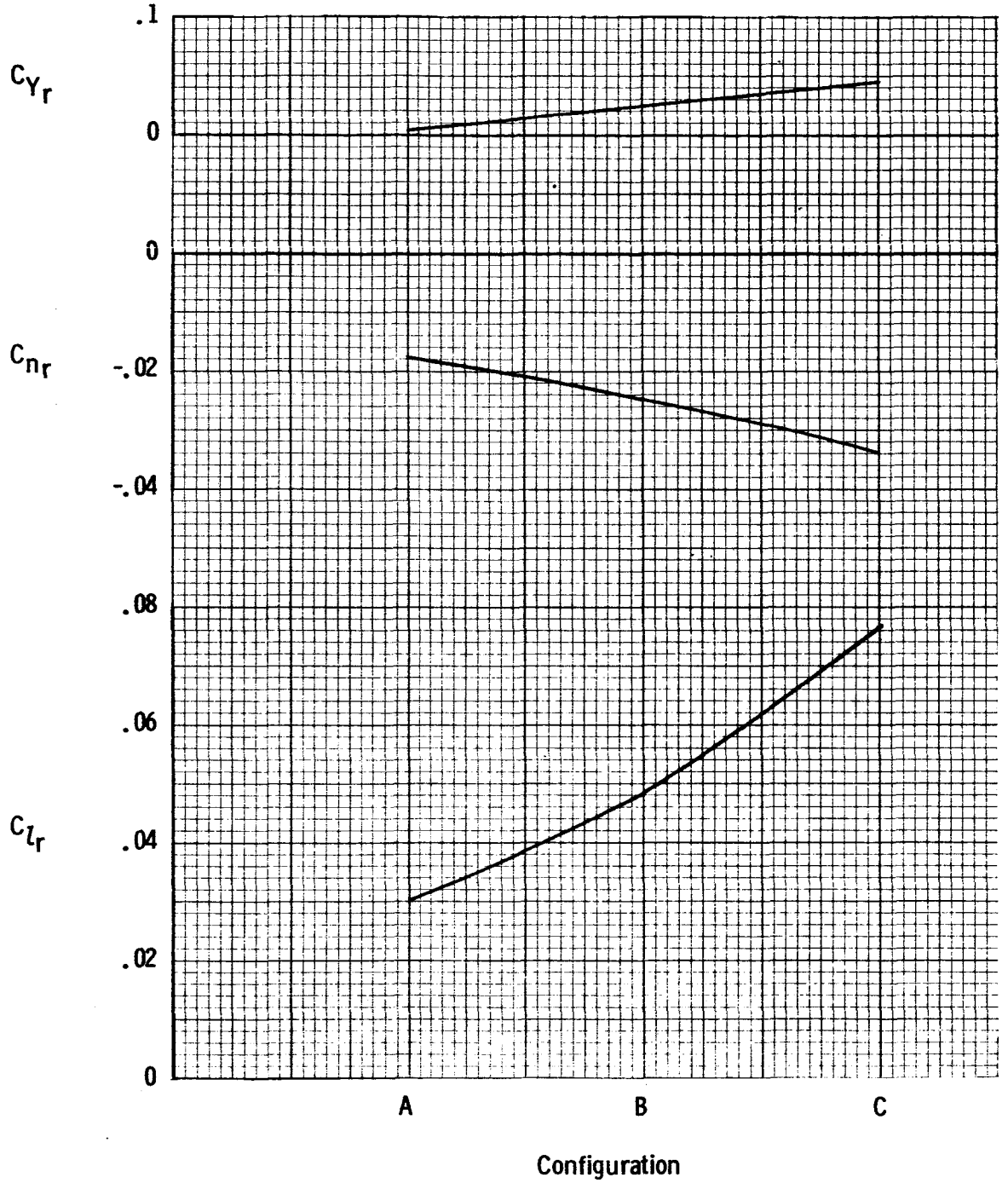

Figure 11.- Variation of the yawing lateral stability derivatives with center-of-gravity position.

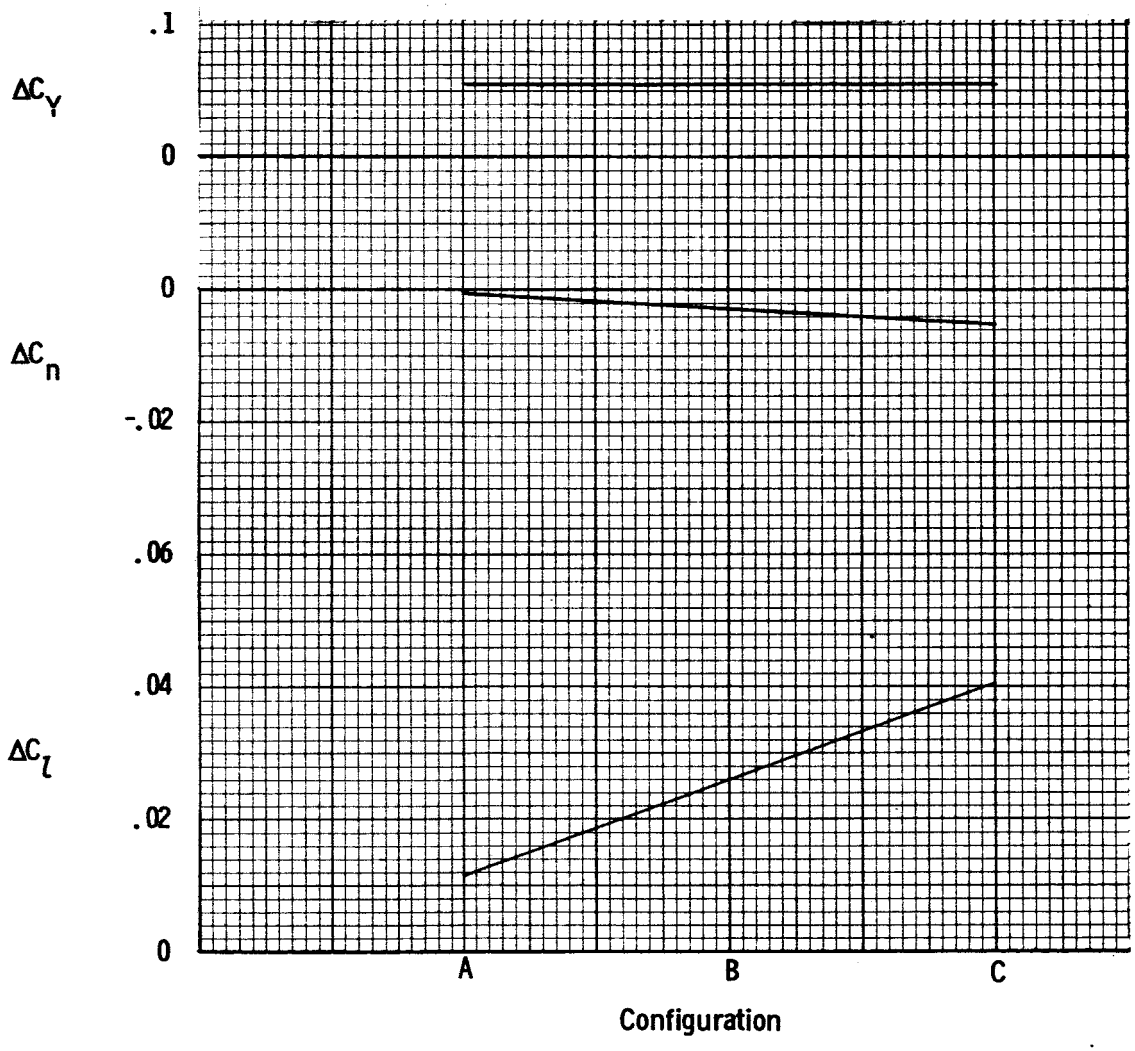

Figure 12.- Incremental values of lateral force and moment coefficients produced by 5° wing-bank angle.

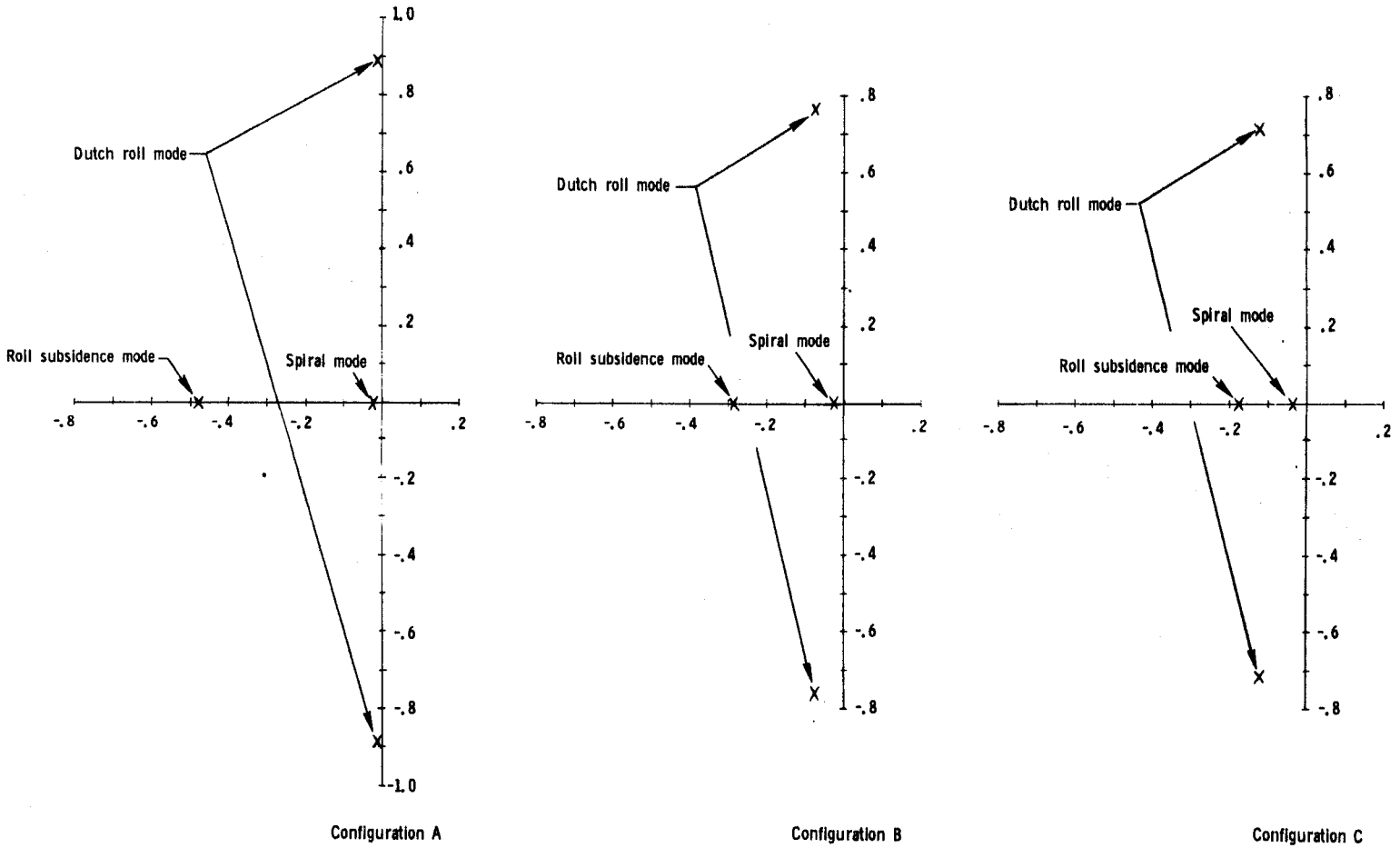

Figure 13.- Location of the nondimensional roots of the lateral stability quartic equations on the complex plane.

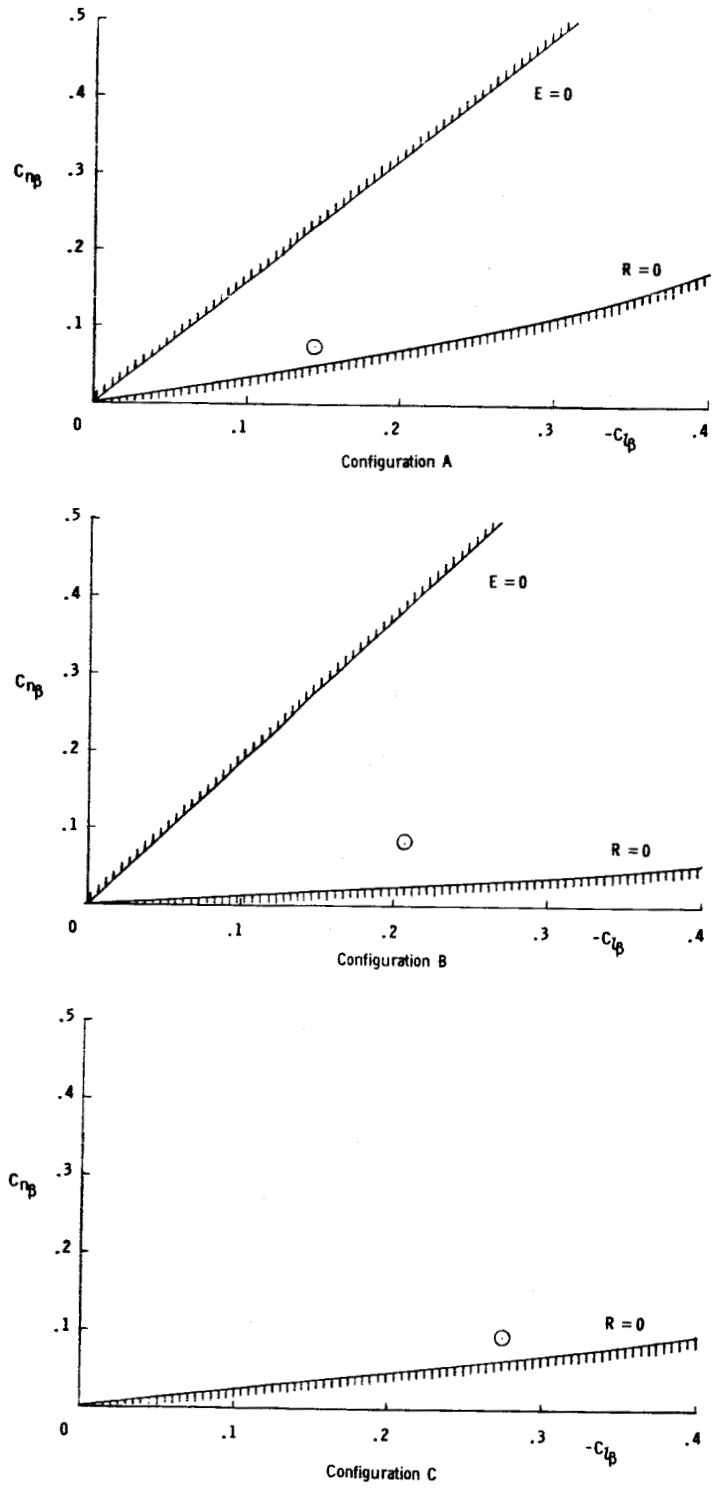

Figure 14.- Stability boundaries for the three configurations.

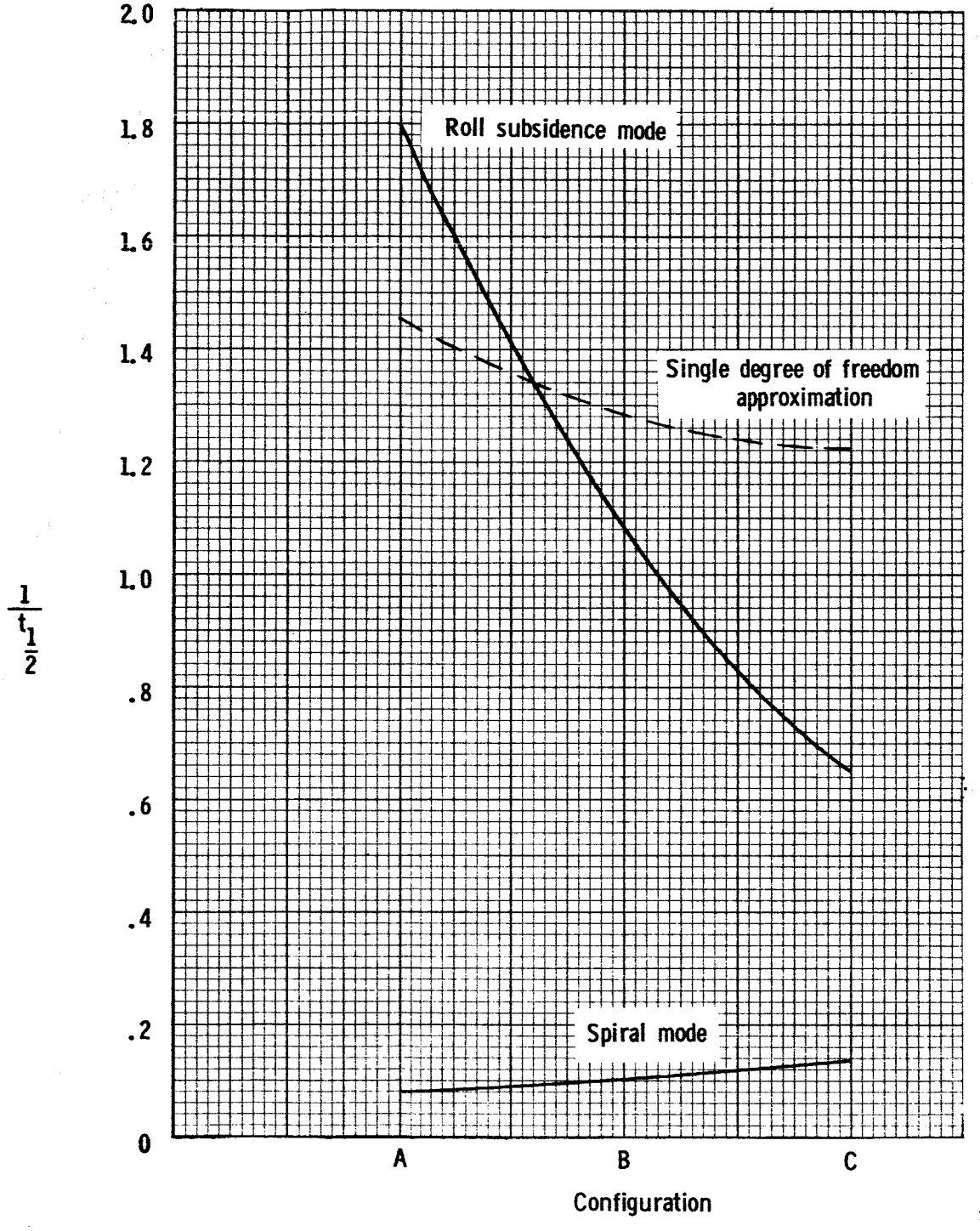

Figure 15.- Variation of the damping factor of the lateral aperiodic modes with center-of-gravity position.

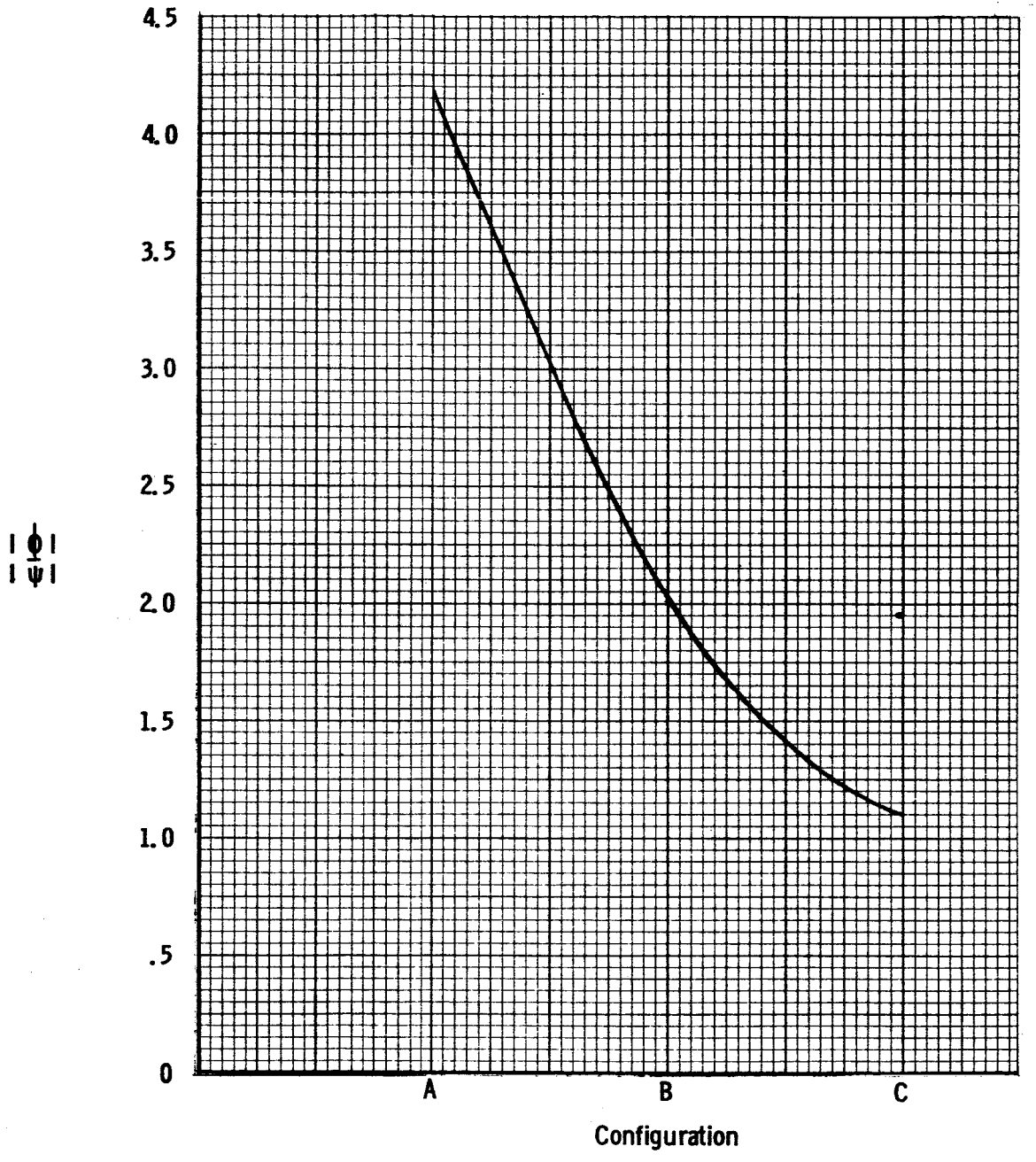

Figure 16.- Variation of the roll-yaw ratio of the roll subsidence mode with center-of-gravity position.

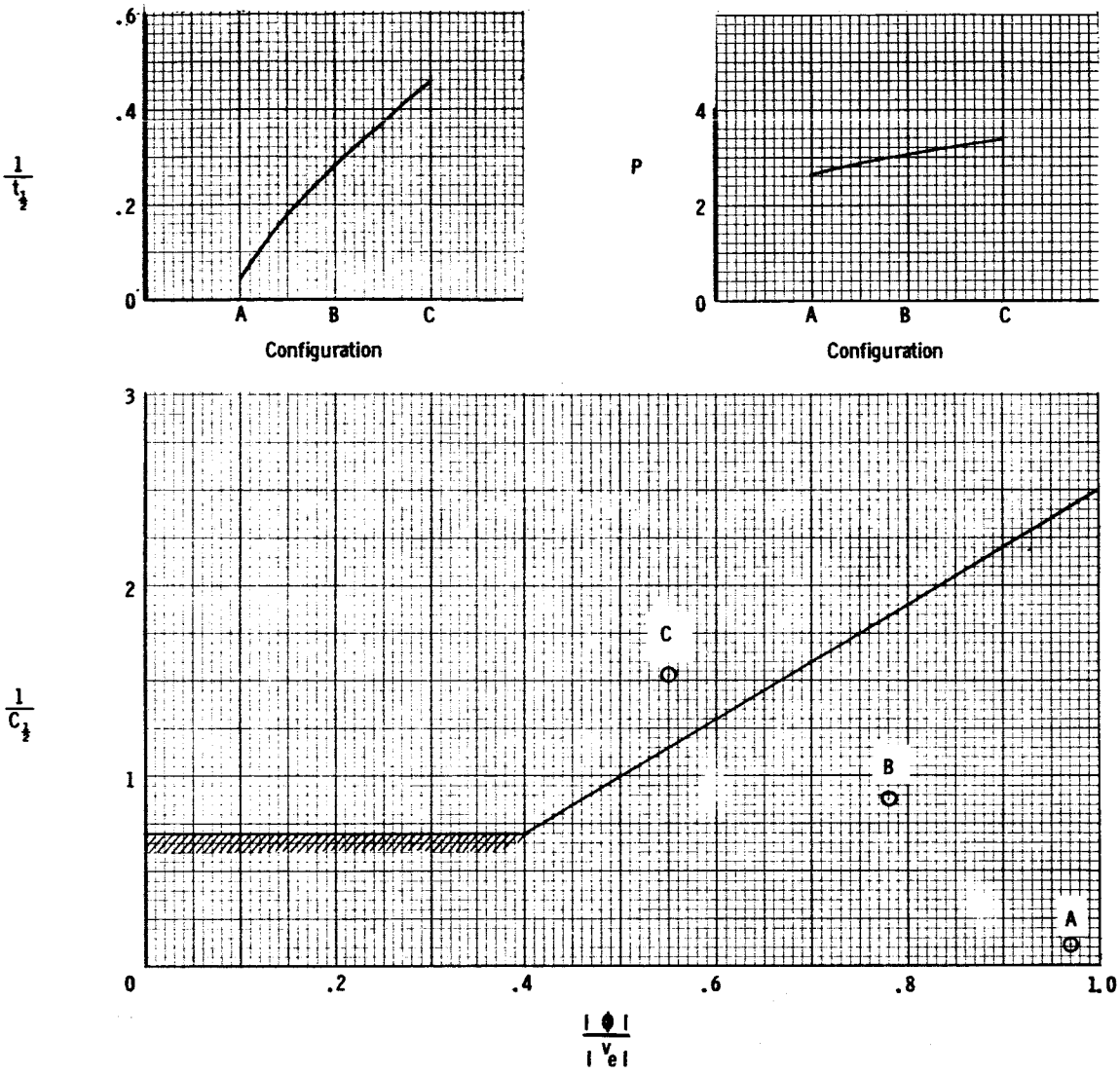

Figure 17.- Summary of the lateral oscillatory characteristics of the three configurations compared with the present military requirements for satisfactory aircraft handling qualities.

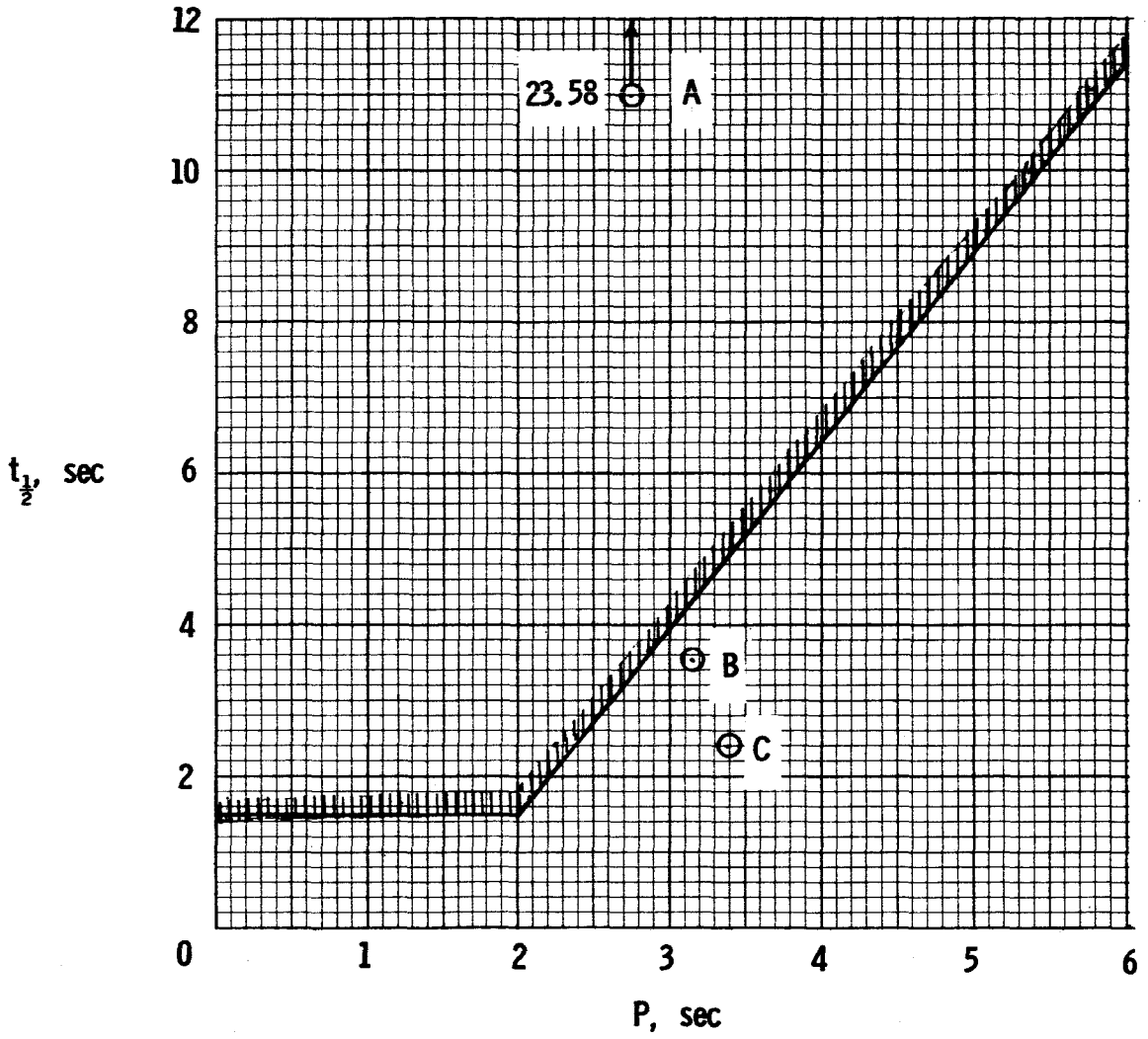

Figure 18.- Oscillatory characteristics compared with the older military handling quality requirements.

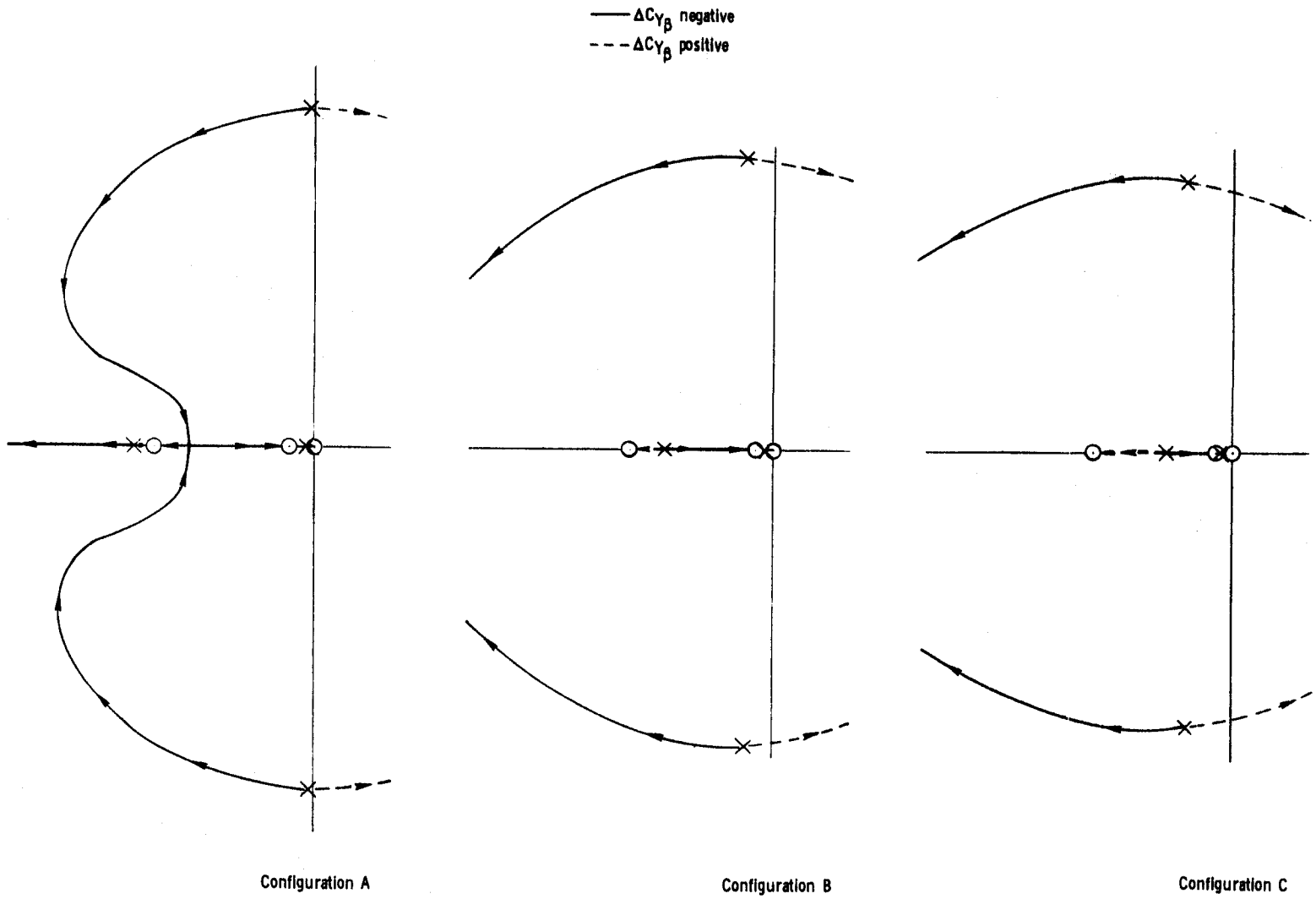

Figure 19.- Root locus sketches for variations of C_{Y_β}.

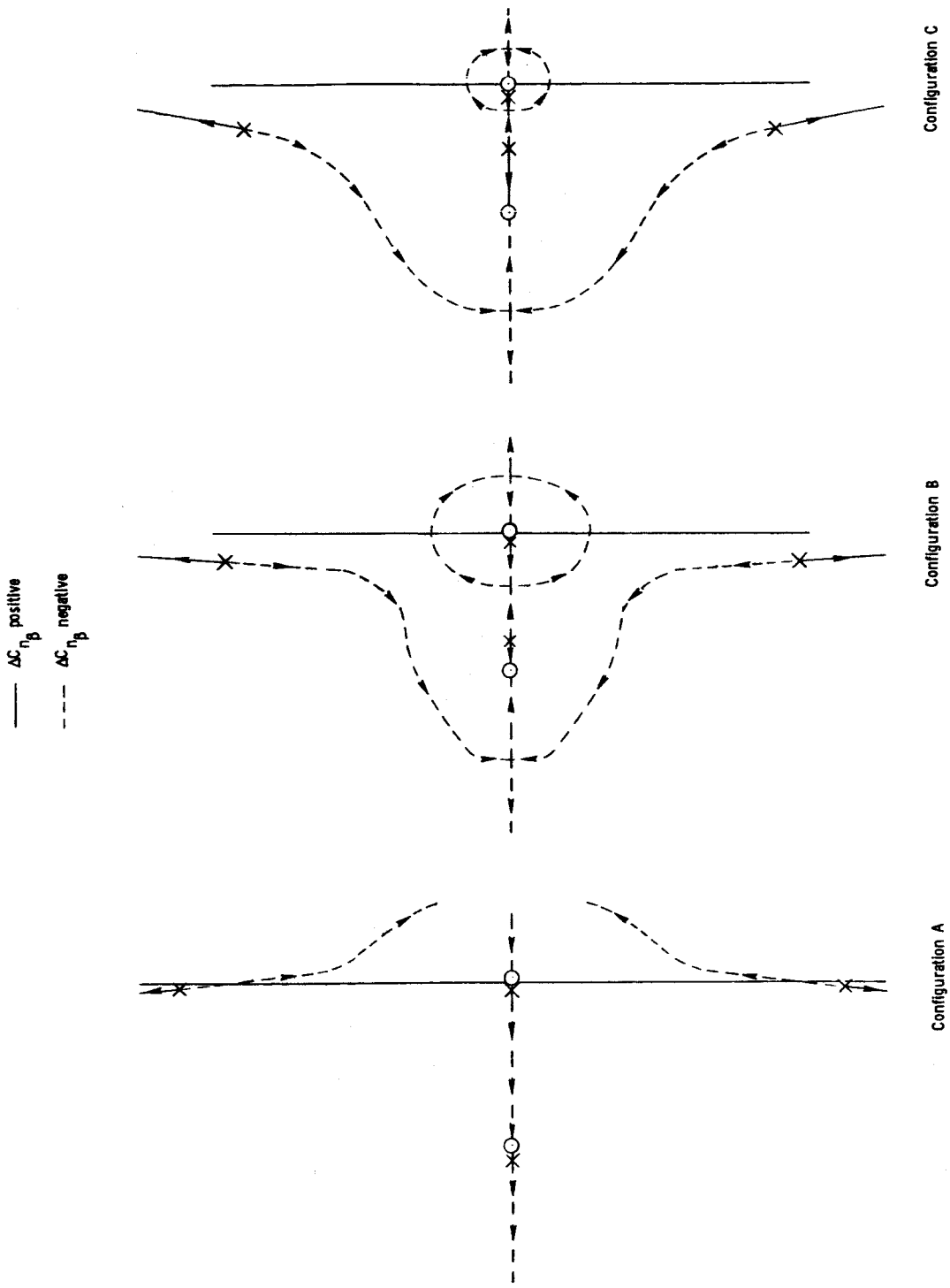

Figure 20.- Root locus sketches for variations of C_{n_β}.

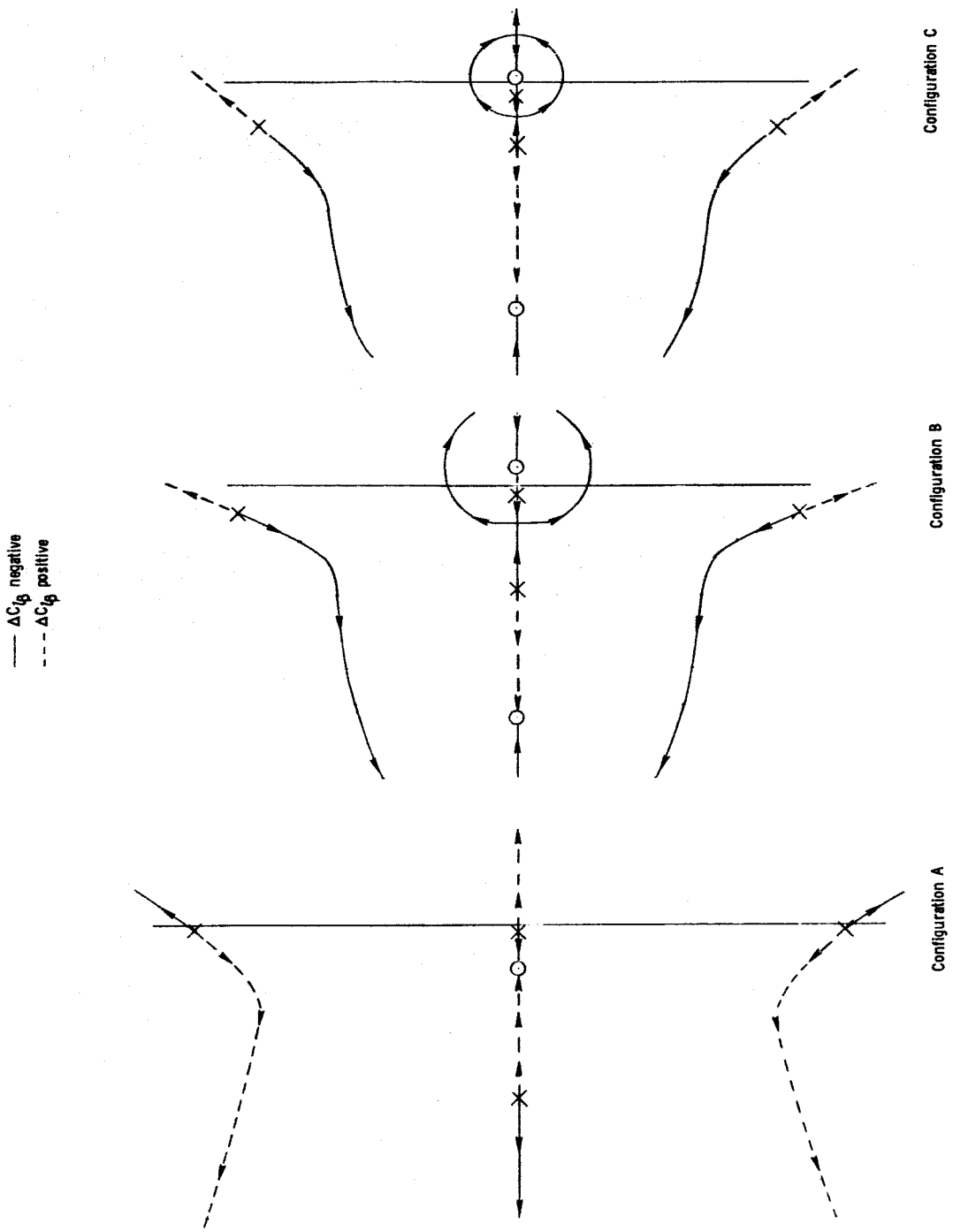

Figure 21.- Root locus sketches for variations of C_{l_β}.

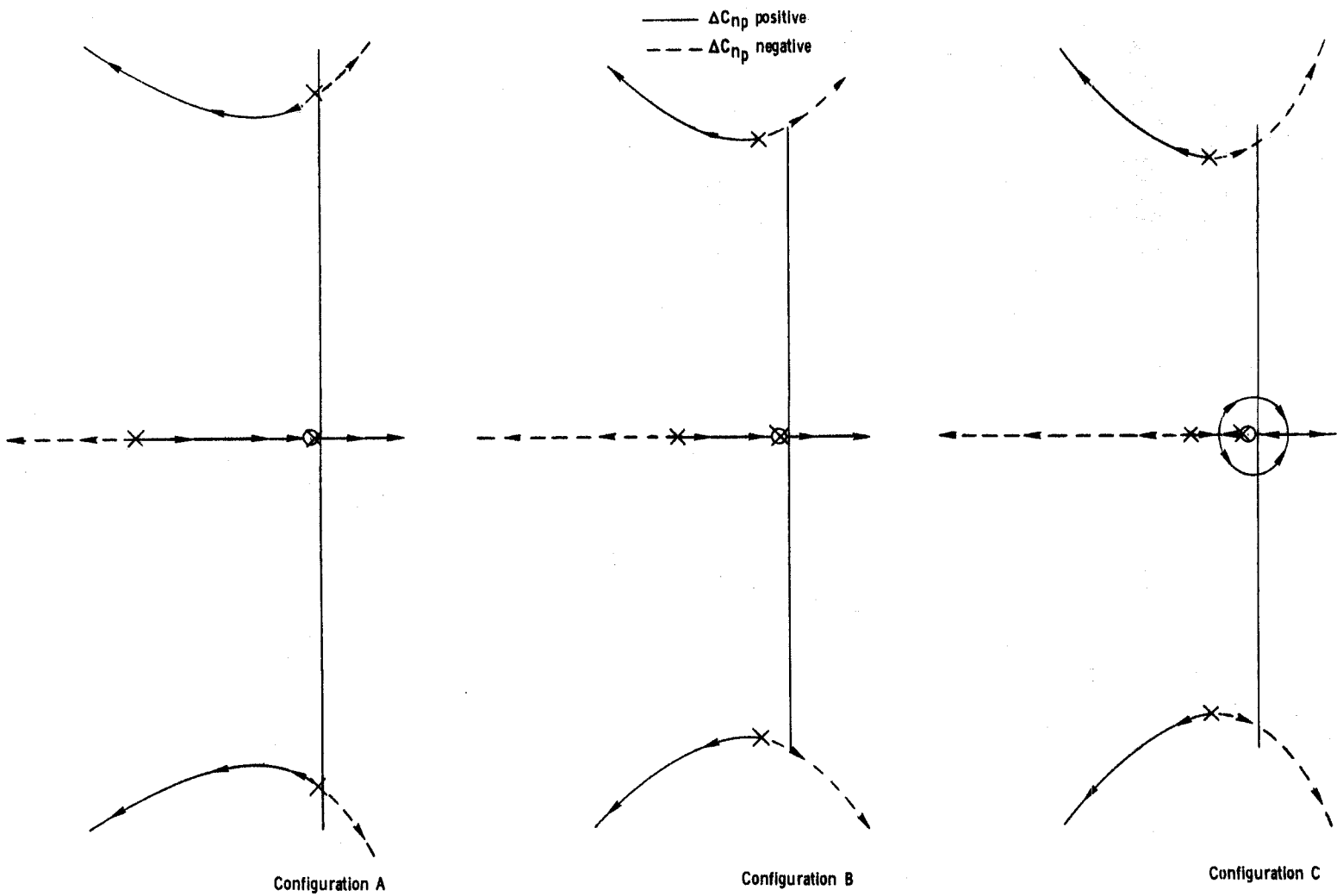

Figure 22.- Root locus sketches for variations of C_{n_p}.

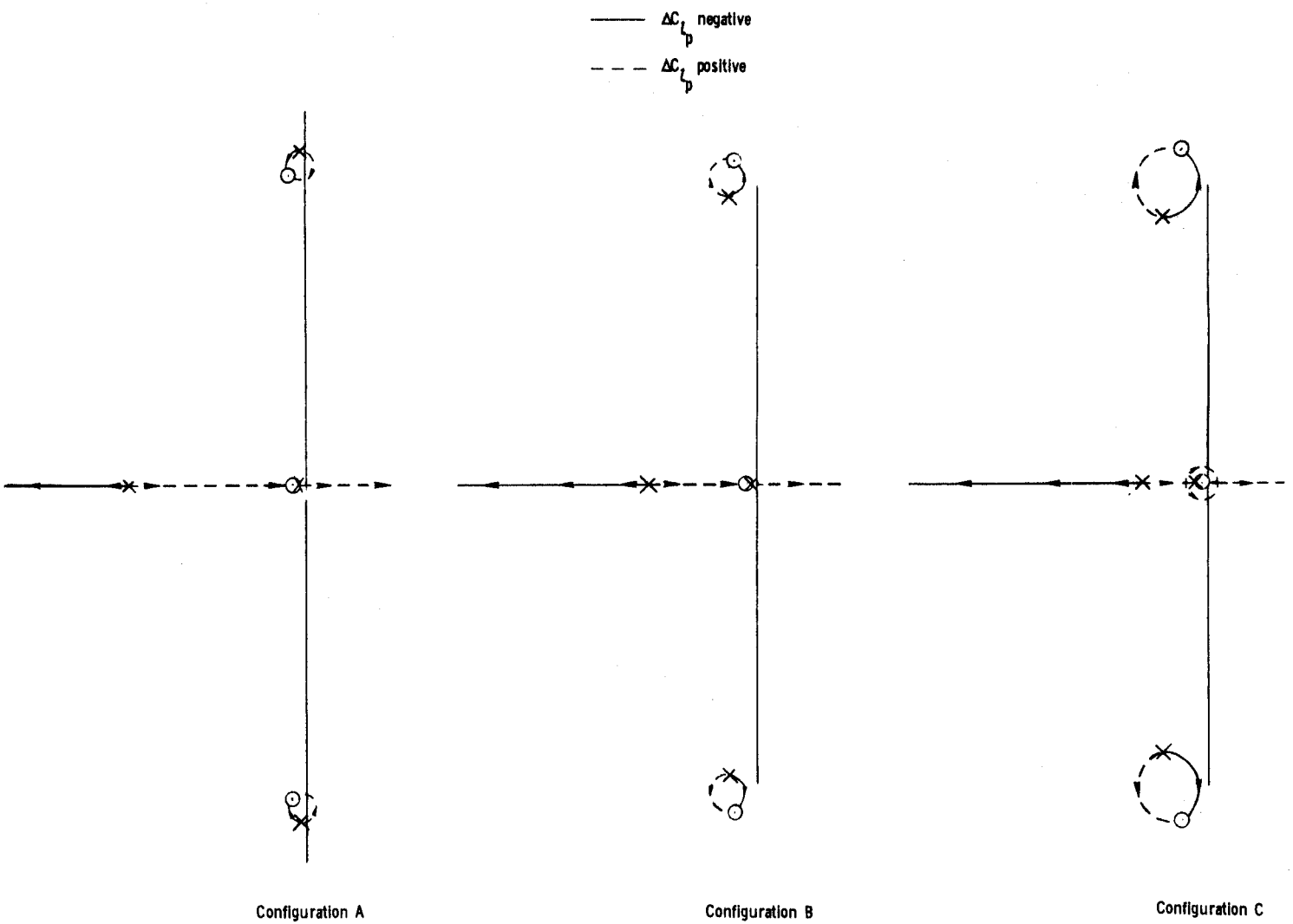

Figure 23.- Root locus sketches for variations of C_{l_p}.

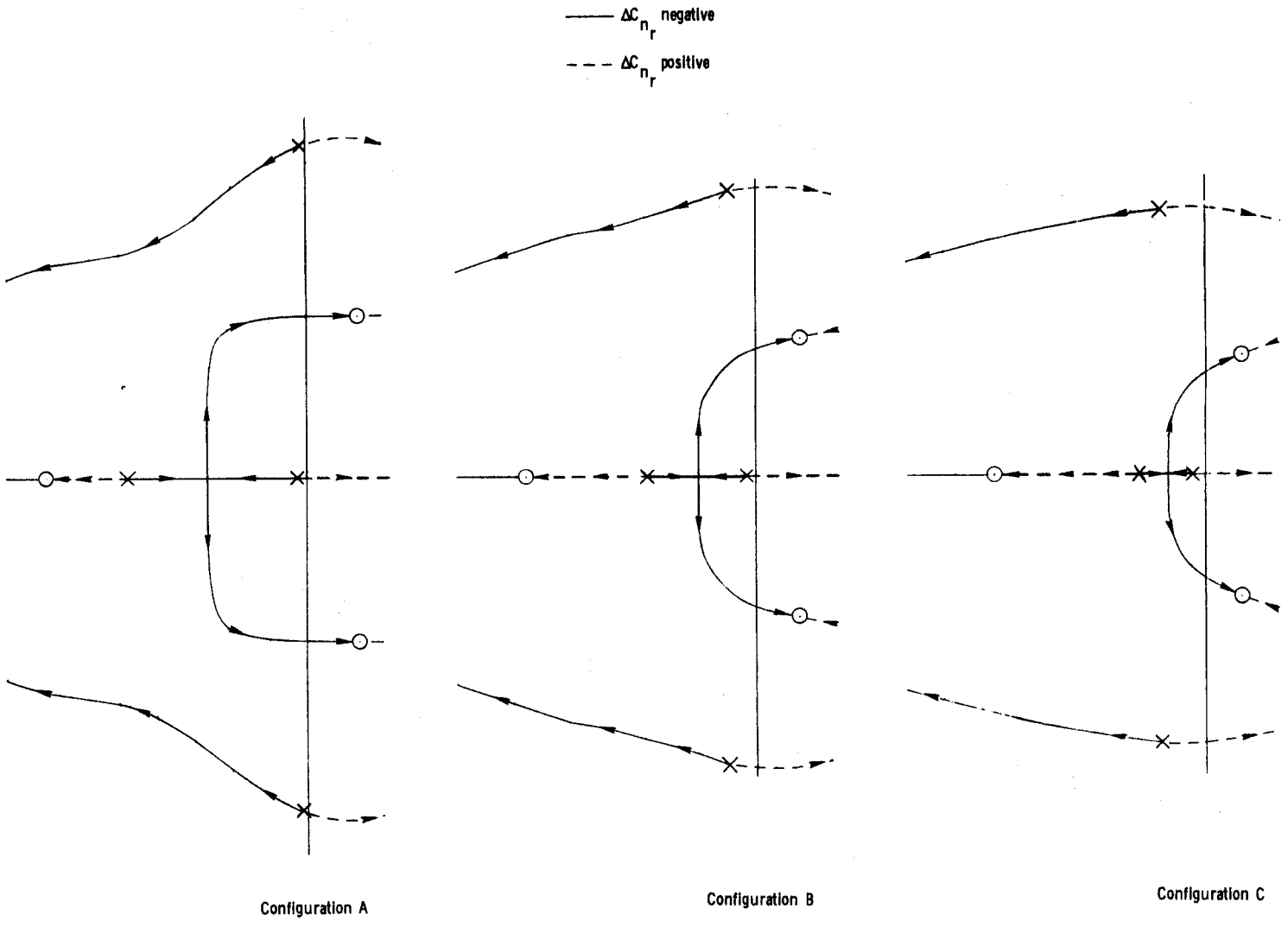

Figure 24.- Root locus sketches for variations of C_{n_r}.

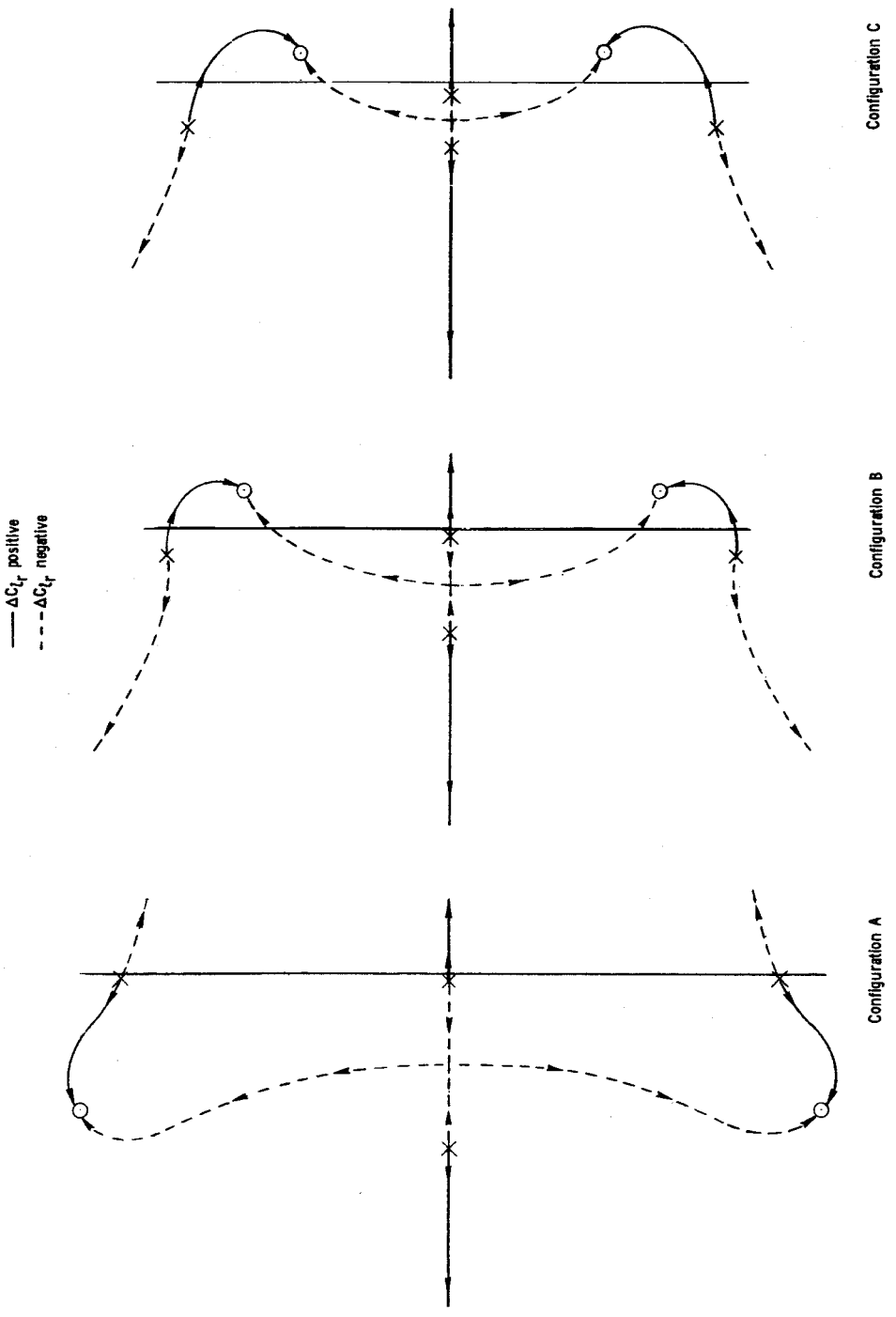

Figure 25.- Root locus sketches for variations of C_{l_r}.

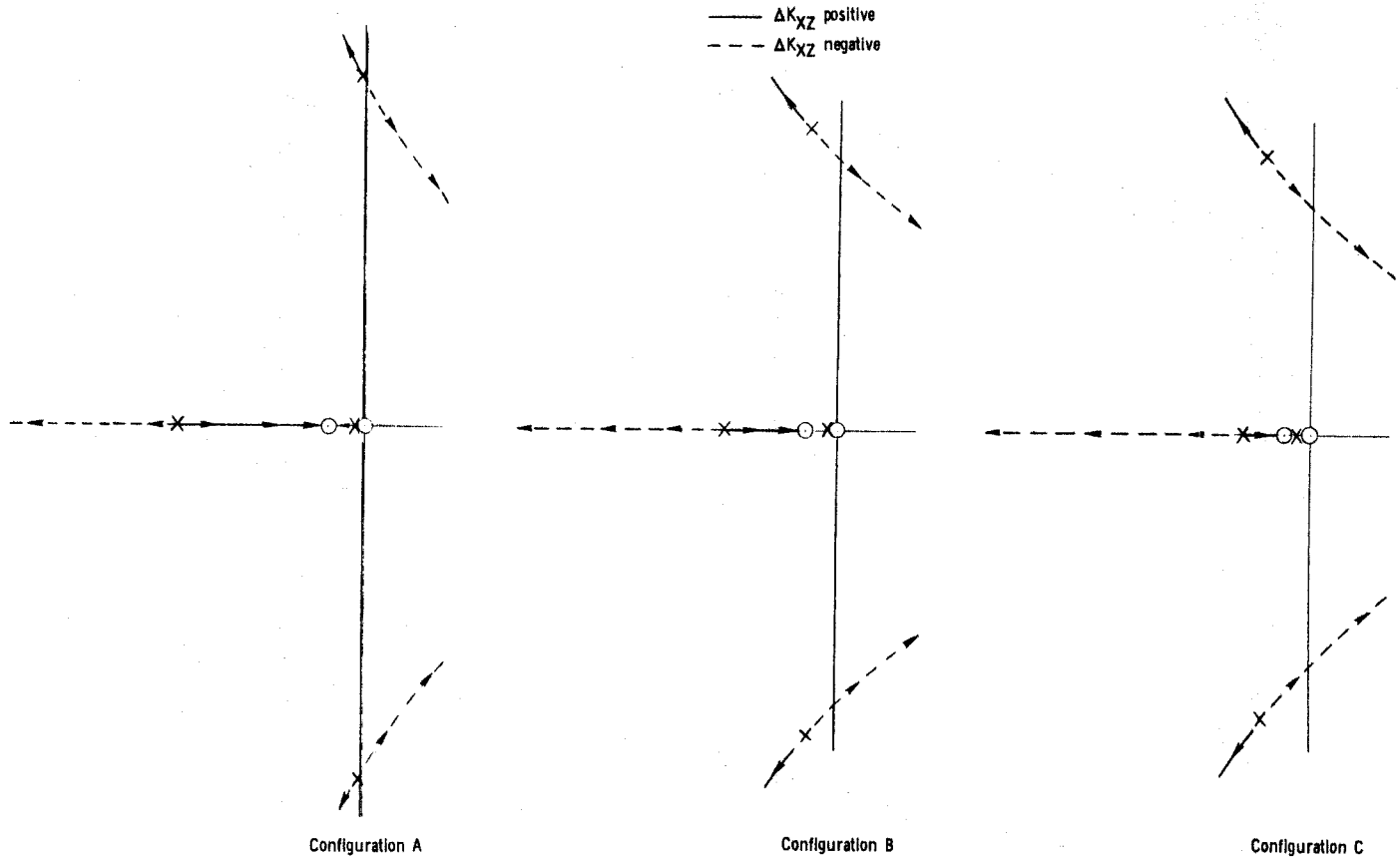

Figure 26.- Root locus sketches for variations of K_{XZ}.

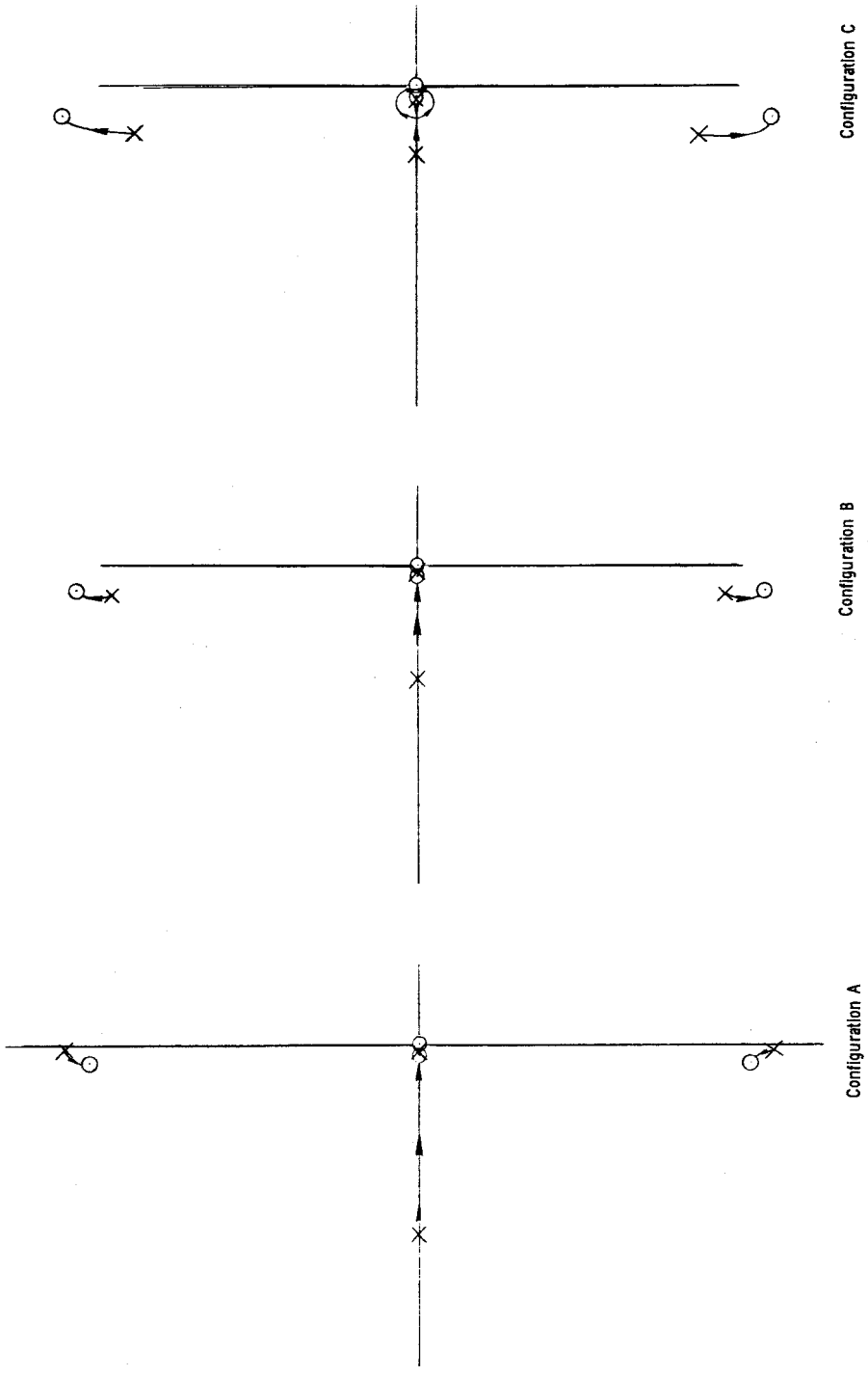

Figure 27.- Root locus sketches for increases in K_X.

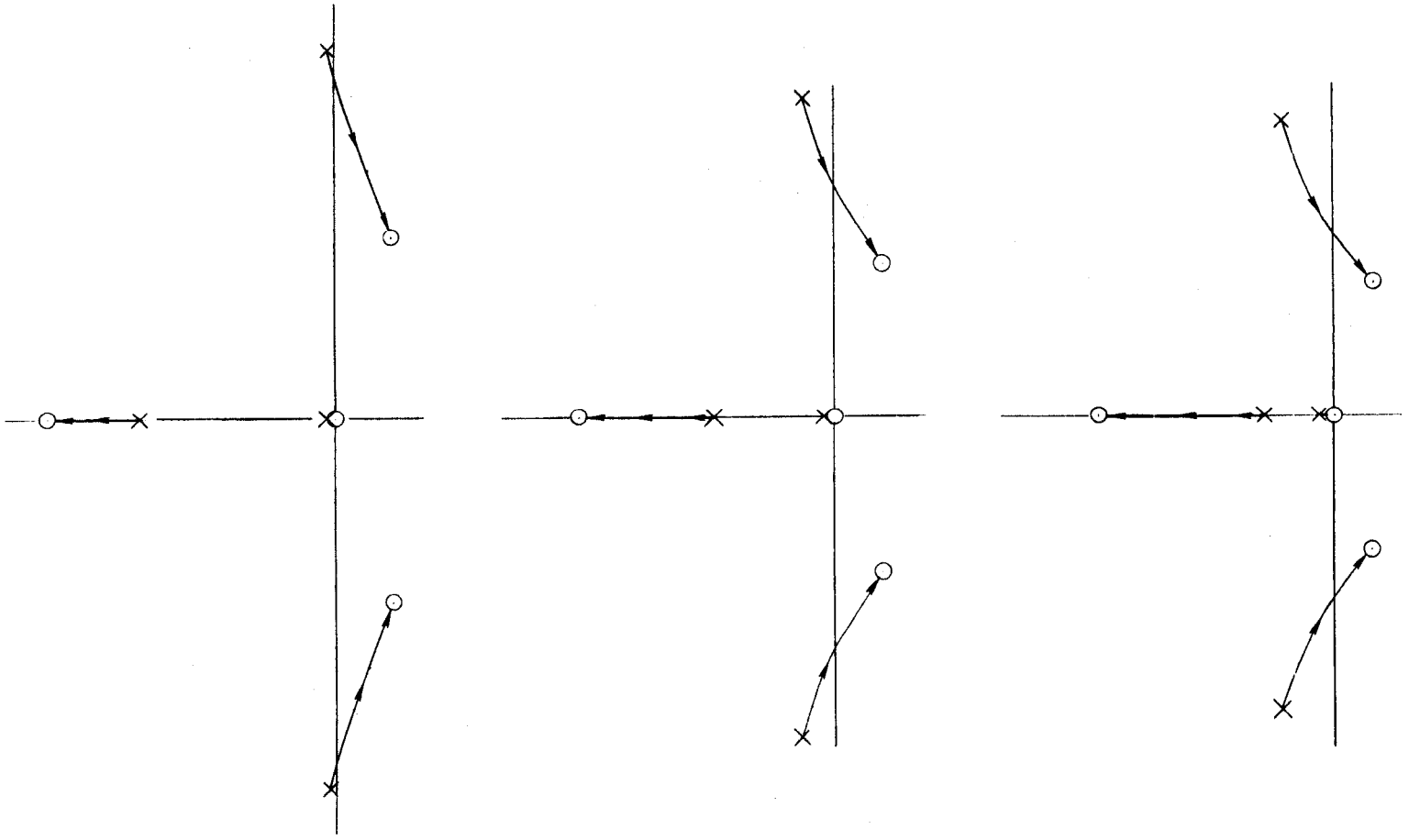

Figure 28.- Root locus sketches for increasing values of K_Z.

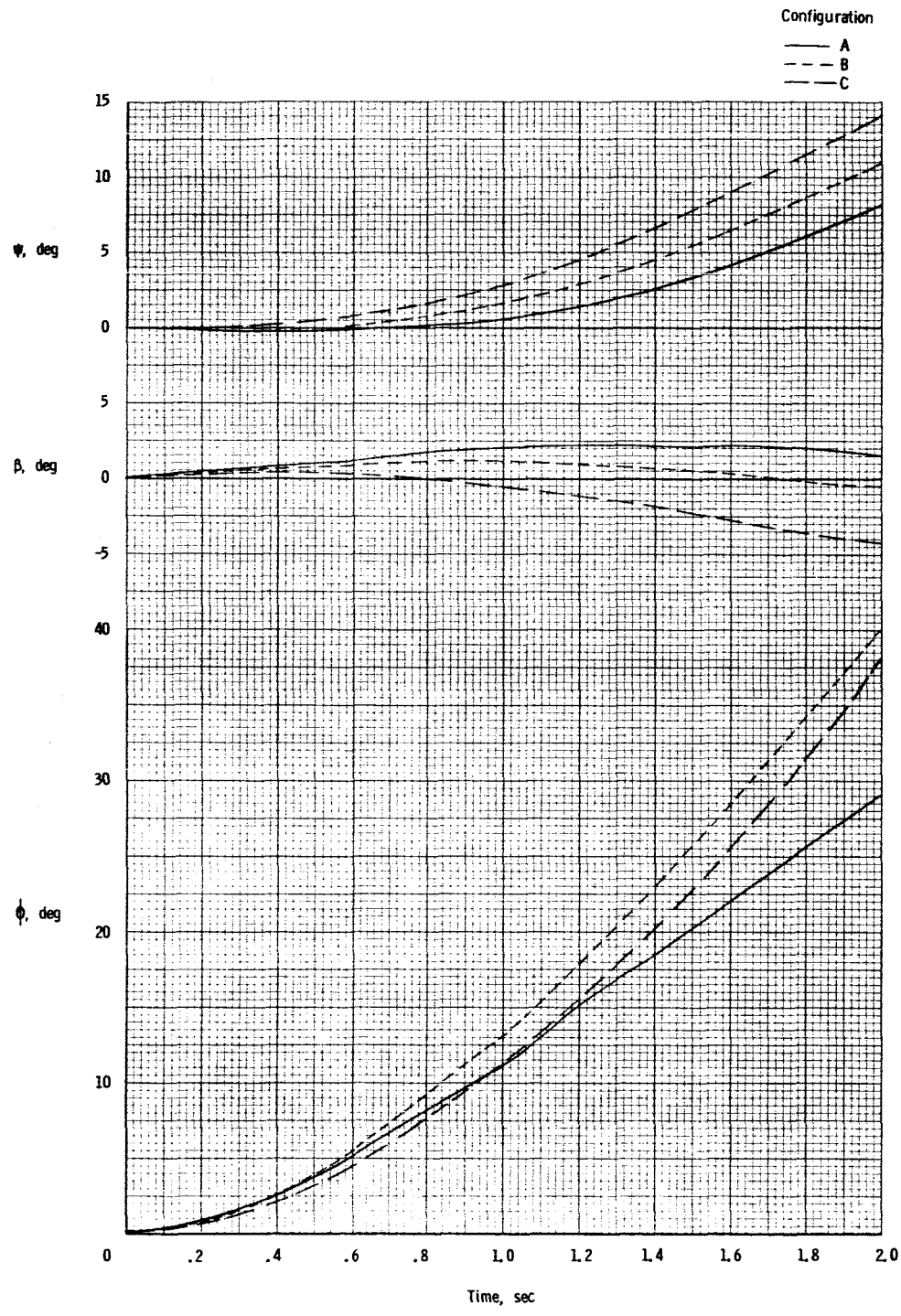

Figure 29.- Effect of center-of-gravity location on lateral response to wing-bank control. $\phi_W = 5^\circ$.

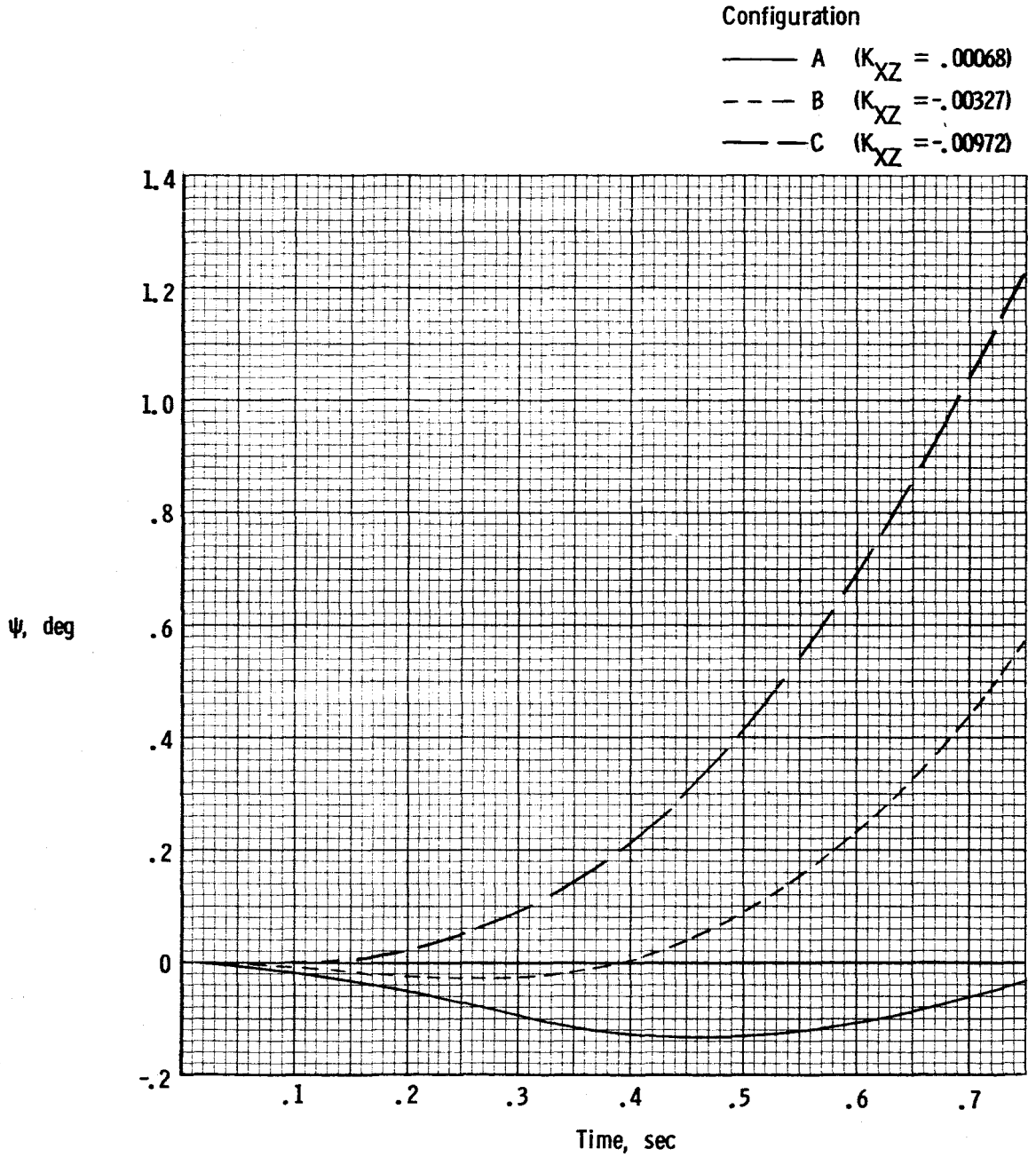

Figure 30.- Effect of center-of-gravity location on initial yawing motion of lateral response.